https://doi.org/10.5194/wes-2026-216
Preprint. Discussion started: 26 November 2026
© Author(s) 2026. CC BY 4.0 License.



eawe european academy of wind energy
Open Access WIND ENERGY SCIENCE DISCUSSIONS

The Role of Surface Representation in Nested Large-Eddy Simulations over Complex Terrain of Perdigão

Dania Al Oqaily[1], Paolo Giani[2], and Paola Crippa[1]

[1]Department of Civil and Environmental Engineering and Earth Sciences, University of Notre Dame, Notre Dame, IN 46556, USA
[2]Department of Earth, Atmospheric and Planetary Sciences, Massachusetts Institute of Technology, Cambridge, MA 02139, USA

Correspondence: Dania Al Oqaily (daloqail@nd.edu) and Paola Crippa (pcrippa@nd.edu)

Abstract.

Accurate representation of land-surface properties is crucial for improving boundary-layer flow simulation in complex terrain. In this study, we investigate whether observationally constrained surface properties can improve the performance of nested large eddy simulations (LES) of the Weather Research and Forecasting (WRF) model over the Perdigão field site. Four WRF-LES runs, driven by realistic boundary conditions, are conducted over the Perdigão field site to decouple the roles of vertical grid configuration, surface roughness length (z_0), and land-use representation. A control (CTRL) run with default land use properties, a run with a coarser vertical grid (CTRL-N_z), an observation-constrained z_0 run (CTRL-z_0-N_z), and a simulations where more realistic representation of the forested landscape through changes in z_0, albedo, and leaf area index (LAI) are implemented (MOD). z_0 is estimated from flux-tower observations using Monin–Obukhov similarity theory and incorporated into WRF-LES. Model results are evaluated against tower, radiosonde, and lidar observations collected during a four-day dry period of the Perdigão 2017 field campaign. Results show that increasing z_0 substantially reduces the RMSE of simulated wind speeds along ridges and within the lower boundary layer, while changes in the vertical-grid configuration have a smaller influence. The MOD configuration reproduces key flow features, including reduced wind magnitudes, enhanced turbulence, and recirculation zones. Although larger errors persist during stable nighttime conditions, MOD better captures the low-level jet and its interaction with the double-ridge topography. Changes in surface representation specifically enhanced of z_0 with lower albedo increasing absorbed shortwave radiation and net radiation. These findings demonstrate that improving the representation of surface properties, particularly aerodynamic z_0, can substantially enhance the performance of nested WRF-LES simulations over forested complex terrain. They highlight the value of observational constraints on land-surface parameters for high-resolution wind simulations, with implications for wind-energy assessment.

1 Introduction

The advancement of computational resources in recent years has enabled numerical weather prediction models to operate at much higher spatial resolutions, allowing real-case simulations to be performed with Large-Eddy Simulations (LES). LES explicitly resolve the dominant turbulent motions in three dimensions and provide valuable insights into how turbulence inter-

https://doi.org/10.5194/wes-2026-216
Preprint. Discussion started: 26 November 2026
© Author(s) 2026. CC BY 4.0 License.



eawe european academy of wind energy
Open Access WIND ENERGY SCIENCE DISCUSSIONS

acts with surface features such as hills, forests, and urban areas (Shaw and Schumann, 1992; Al Oqaily et al., 2025; Tamura et al., 2007; Auvinen et al., 2020). For real-case atmospheric simulations, LES domains are commonly nested within coarser-resolution mesoscale domains, allowing large-scale meteorological conditions to drive the development of finer-scale turbulent structures. However, the accuracy of these multiscale simulations depends on several model configuration choices, including the representation of surface characteristics. As the model grid spacing decreases to tens or hundreds of meters, the representation of surface obstacles becomes increasingly important (Wagner et al., 2019b; Aumond et al., 2013). The Weather Research and Forecasting (WRF) model typically assigns predefined surface parameters based on the dominant land-use category, including aerodynamic surface roughness (z_0). However, at high resolutions, features such as forests become increasingly important relative to the model grid spacing, making simulations sensitive to their representation through land-surface parameterizations. Improving the representation of these effects, including vegetation-induced drag, is particularly important for simulating boundary-layer winds, which are crucial for wind-energy assessments in complex and forested terrain (Fang et al., 2018; Adedipe et al., 2020; Agafonova, 2017).

A positive near-surface wind bias over land has been widely reported in the WRF model (Jiménez et al., 2012; Lee et al., 2023; Wagner et al., 2019b; Quimbayo-Duarte et al., 2022; Solbakken et al., 2021; Al Oqaily et al., 2025; Janiszeski and Crippa, 2025), motivating efforts to reduce this systematic bias. Several studies have proposed approaches to reduce this overestimation, resulting in significant improvements in simulation performance. Dupont and Brunet (2008) demonstrated that incorporating vegetation effects through a drag-force approach in LES enables realistic simulation of turbulent flows within and above forest canopies, validated against wind tunnel measurements. Similarly, Liu et al. (2016) used LES to investigate vegetation drag effects over complex terrain, showing that adding friction or drag terms in the momentum equations accurately reproduces turbulence characteristics in both idealized and real forested terrains. Building on these concepts, Wagner et al. (2019b) performed long-term WRF simulations with a forest parameterization based on the drag-force approach, reporting good agreement with observations. Quimbayo-Duarte et al. (2022) further compared high-resolution simulations with and without the forest parameterization during the Perdigão 2017 field campaign and found that including the forest parameterization resulted in closer agreement with observations of the low-level jet (LLJ) and near-surface flow, particularly the recirculation zones near the slopes. Similarly, Venkatraman et al. (2023) investigated the influence of forest canopy representation and inflow conditions on simulated flow over the Perdigão site using Reynolds-averaged Navier–Stokes simulations, emphasizing the importance of accurately representing canopy-induced drag, wind profiles, and flow recirculation for reliable wind-resource assessment in complex terrain. Finally, Lee et al. (2020) developed a new surface-layer scheme in WRF that explicitly accounts for the roughness sublayer, where the Monin– Obukhov Similarity Theory (MOST) breaks down. Their evaluation showed that this scheme enhances the representation of surface processes and vertical turbulent transport, effectively reducing the common overestimation of surface wind speeds, especially over areas with tall vegetation and low Leaf-Area-Index (LAI), while incurring only a small computational cost. The importance of accurately representing land surface properties also extends to wind-energy applications, as uncertainties in z_0 can propagate into wind-speed predictions and wind-resource estimates (Kelly and Jørgensen, 2017). Beyond their influence on wind patterns, land surface characteristics, such as orography, land cover, soil moisture, and vegetation, critically shape energy partitioning, moisture fluxes, and local circulation (Bonan et al., 2018).

https://doi.org/10.5194/wes-2026-216
Preprint. Discussion started: 26 November 2026
© Author(s) 2026. CC BY 4.0 License.



eawe european academy of wind energy
Open Access WIND ENERGY SCIENCE DISCUSSIONS

Accurate representation of surface parameters, including albedo, z_0, and soil properties, is therefore essential for realistic fine-scale predictions of surface fluxes which strongly influence land–atmosphere interactions and climate. Numerous studies show that using high-resolution, up-to-date land-use data improves model performance, highlighting the importance of continuously refining surface datasets and parameterizations to better represent these interactions (Pineda et al., 2004; De Meij et al., 2009; Sertel et al., 2010; Schicker et al., 2016).

Previous studies have highlighted the sensitivity of global-to-LES nested simulations to the representation of static surface characteristics. In particular, Giani and Crippa (2024) demonstrated that the choice of surface datasets, including topography and land-use classification, can substantially influence simulated wind fields, with sensitivities that may exceed those associated with turbulence parameterizations, LES subgrid-scale closures, and initial and boundary conditions. These findings emphasize that increasing spatial resolution alone does not necessarily improve model performance if the underlying surface characteristics are not adequately represented. However, an important question remains whether observationally constrained adjustments to surface parameters canimprove the performance of nested WRF-LES simulations. This is particularly relevant over forested complex terrain, where land-use datasets may underestimate z_0 and consequently affect the simulated momentum exchange between the surface and atmosphere.

Building on these findings, we investigate whether improving the representation of land-surface properties can enhance the performance of mesoscale-to-LES nested WRF simulations over the Perdigão field site. We first estimate z_0 from flux tower observations using MOST. Although the MOST-derived roughness length is subject to uncertainty due to complex terrain and canopy effects, the observational estimates indicate that the default value of approximately 0.1 m substantially underrepresents the z_0 of the forested Perdigão site. We then conduct a series of numerical simulations with WRF-LES to assess the sensitivity of atmospheric properties to land-surface characteristics and vertical-grid configuration on simulated boundary-layer flow within the context of the Perdigão 2017 field campaign. The control simulation uses the default WRF surface parameters, while additional sensitivity experiments modify the vertical grid configuration and z_0. A final experiment combines both the observed z_0 and a more realistic land-use category consistent with the forest conditions observed at the site. Rather than introducing an explicit canopy-drag parameterization, we investigate whether adjustments to surface properties within the standard WRF-LES framework can improve agreement with atmospheric observations from the Perdigão 2017 field campaign. This work specifically aims to:

1. Integrate high-resolution flux tower observations to improve the representation of surface properties in nested WRF-LES, enhancing simulation of boundary-layer flow over complex terrain.

2. Evaluate how change to realistic land-surface representation influence boundary-layer dynamics in LES, including near-surface and aloft wind fields, turbulence intensity, and recirculation patterns.

3. Quantify the relative contributions of vertical grid configuration, z_0, and land-use representation to the performance of nested WRF-LES, and assess how the modified surface properties influence the surface energy budget.

https://doi.org/10.5194/wes-2026-216
Preprint. Discussion started: 26 November 2026
© Author(s) 2026. CC BY 4.0 License.



eawe european academy of wind energy
Open Access WIND ENERGY SCIENCE DISCUSSIONS

The remainder of this paper is organized as follows. Section 2 describes the study area, observational data, and the method used to estimate z_0, followed by details of the numerical simulation ensemble. Section 3 presents and discusses the results, while Section 4 summarizes the main findings and provides the overall conclusions.

2 Materials and Methods

2.1 Observational Data

In this study, measurements from the Integrated Surface Flux System (ISFS) meteorological towers installed in the Perdigão area and distributed on two parallel ridges aligned northwest to southeast—separated by a ∼1.5 km-wide valley—and a transect in the prevailing wind direction (Figure 1c, pink square) are used to estimate the z_0 locally, as described in Section 2.2. These measurements consist of eddy flux tower data, including mean wind speed at 10 m with its horizontal and vertical fluctuations, as well as sonic temperature fluctuations used to infer heat fluxes. The Perdigão experiment featured an extensive instrumentation suite, and a complete overview is available in (Fernando et al., 2019). In-situ observations used in this study include the quality-controlled 5-minute tower data at 45 locations provided by the National Center for Atmospheric Research Earth Observing Laboratory (UCAR/NCAR - Earth Observing Laboratory, 2019). The analysis focuses on the period from 19 May 00:00 UTC to 23 May 00:00 UTC, corresponding to the simulation period.

Measurements of horizontal wind speed and potential temperature at the meteorological towers are used to quantify the model bias in the WRF-LES simulations described in Section 2.3. Air temperature is converted to potential temperature using the relation $\Theta = T\left(\frac{p_0}{p}\right)^{R/c_p}$, where T is the temperature at each specific elevation (10m and 100m), p is the pressure, p_0 is the reference pressure, R is the gas constant, and c_p is the specific heat at constant pressure (with $R/c_p = 0.286$). Only three towers provide measurements at multiple altitudes above ground level (AGL), ranging from 2 m to 100 m, shown as stars in Figure 1c. Radiosonde data, launched daily at 0510 UTC from a valley site, offer vertical wind speed profiles for evaluating the simulations with and without the z_0 modification. Four DTU Doppler wind Light Detection and Ranging (lidars) (WS1–WS4; (Wagner et al., 2019b)) scanned across the double ridge parallel to the prevailing wind direction. WS1 and WS3 were oriented southwest (azimuth 234.68°), while WS2 and WS4 scanned northeast (azimuth 54.68°). WS2 and WS3 are not shown in Figure 1c because they were located close to WS1 and WS4, respectively. The combination of the four lidars enabled the construction of composite radial velocity fields perpendicular to the double ridge, which were used to assess the low-level jet (LLJ) on 22 May at 04:01:09 UTC.

For the surface energy budget calculations, only three towers—rne01, rsw04 (located over the ridge), and v04 (located in the valley)—provided surface radiation measurements (yellow circle). These data were used to validate differences between the two configurations, with and without modified land-surface properties.

https://doi.org/10.5194/wes-2026-216
Preprint. Discussion started: 26 November 2026
© Author(s) 2026. CC BY 4.0 License.



eawe european academy of wind energy
Open Access WIND ENERGY SCIENCE DISCUSSIONS

2.2 Surface Roughness Estimation and Diagnostic Methods

2.2.1 Estimation of Aerodynamic Roughness Length

To estimate z_0 and correct the near-surface wind speed, we apply MOST, which provides a robust framework for describing turbulent flow in the atmospheric surface layer. This theory is particularly valuable for linking vertical wind speed profiles to land surface characteristics such as z_0, which directly influences how air moves near the ground (Monin and Obukhov, 1954). Near the surface, wind speed is reduced by frictional drag, which depends on land cover type and its associated z_0. In forests, this effect is represented by a zero-plane displacement height (d), typically 0.6–0.8 times the canopy height, which shifts the wind profile upward so that it fully develops only above the canopy. Below the treetops, the flow is minimal or nearly stagnant, whereas above the canopy large-scale vortices dominate, enhancing turbulence and allowing wind speed to increase more rapidly (Elgendi et al., 2023). Figure S1 illustrates the expected difference in wind speed profiles between an open field and a forest canopy.

In this section, we describe how MOST is used to estimate Z_0 over the analyzed LES domain to improve the fidelity of simulated near-surface wind speeds. The approach relies on ISFS wind speed observations at 10 m during a period of relatively neutral conditions—specifically, from 00 UTC on May 19 to 12 UTC on May 21, when no significant change in synoptic conditions was present. Data from 18 ISFS towers is included in the analysis, based on the availability of all required variables for the calculations. According to MOST, the 10 m observed wind speed (i.e., $U_{O,10}$) can be expressed as:

$$U_{O,10} = \frac{u^*}{k}\left[\ln\left(\frac{10-d}{Z_0}\right) - \psi_m\left(\frac{10-d}{L}\right) + \psi_m\left(\frac{Z_0}{L}\right)\right] \tag{1}$$

where $k = 0.4$ is the von Karman constant, u^* is the friction velocity, ψ_m is the integrated similarity function of the momentum, and L is the Obukhov length. For forest canopies, d is estimated to vary between 0.6 and 0.8 times the height of the canopy (Stull, 2012), where the logarithmic wind profile goes to zero. d can be estimated from Z_0 based on the relationships $Z_0/h = 0.15$ and $d/h = 0.65$, where h is canopy height (Arya, 2001). Therefore, d was assumed as $4.33Z_0$ in our study.

The velocity fluctuations are defined as deviations from their temporal means:

$$u' = u - \overline{u}, \qquad v' = v - \overline{v}, \qquad w' = w - \overline{w}, \tag{2}$$

where u, v, and w are the two horizontal and vertical velocity components, respectively, and the overbar denotes temporal averaging. The velocity variances are expressed as $\overline{u'^2}$, $\overline{v'^2}$, and $\overline{w'^2}$, while the covariances $\overline{u'w'}$ and $\overline{v'w'}$ represent the turbulent momentum fluxes.

Friction velocity (u^*) is calculated using flux tower measurements of the covariances between horizontal and vertical wind fluctuations at 10 m. Using the horizontal Reynolds stress vector, the friction velocity is defined as (Weber, 1999):

$$u^* = \sqrt{\frac{\tau_{hor}}{\rho}} = \left[\left(\overline{u'w'}\right)^2 + \left(\overline{v'w'}\right)^2\right]^{\frac{1}{4}} \tag{3}$$

https://doi.org/10.5194/wes-2026-216
Preprint. Discussion started: 26 November 2026
© Author(s) 2026. CC BY 4.0 License.



eawe european academy of wind energy
Open Access WIND ENERGY SCIENCE DISCUSSIONS

where τ_{hor} is the magnitude of the horizontal turbulent shear stress, and ρ is the mean air density.

The atmospheric stability correction required to estimate z_0 from Eq. 1 is determined using the Obukhov length (L), defined as

$$L = -\frac{u^{*3}\overline{\theta}}{kg\overline{w'\theta'}} \tag{4}$$

where g is the gravitational acceleration, $\overline{\theta}$ is the mean air potential temperature, and $\overline{w'\theta'}$ is the turbulent kinematic potential-temperature flux. Negative and positive values of L indicate unstable and stable atmospheric conditions, respectively, while near-neutral conditions correspond to large absolute values of L.

The turbulent heat flux was estimated from the ISFS sonic-anemometer measurements. The measured covariance between vertical velocity and sonic temperature fluctuations, $\overline{w'T'_c}$, was corrected to estimate the air-temperature covariance, $\overline{w'T'}$, following Schotanus et al. (1983); NCAR (2025). The correction accounts for the influence of humidity on sonic temperature and depends on the Bowen ratio (B). A value of $B = 1.25$ was adopted based on the average daytime ratio of simulated sensible (H) to latent heat flux (LE) during the study period, as direct observations of these fluxes were unavailable. A sensitivity analysis showed that the resulting mean z_0 estimates differed by less than 1% over the tested range of B.

The corrected air-temperature covariance, $\overline{w'T'}$, was used to calculate L, approximating the potential-temperature covariance $\overline{w'\theta'}$ in Eq. 4. The resulting L was then used to determine the momentum stability correction ψ_m in Eq. 1. The aerodynamic roughness length (z_0) was subsequently estimated using the observed wind speed and friction velocity, together with the assumed displacement-height relationship $d = 4.33 z_0$.

This approach was applied to all tower locations with available $U_{O,10}$ measurements over the four analyzed days, using 5-min averaged observational statistics and excluding the period influenced by synoptic conditions (12:00 UTC on May 21 to 06:00 UTC on May 22). The spatially averaged z_0 was approximately $1.87\,\mathrm{m}$. To assess the sensitivity of the estimated z_0 to the averaging period, the analysis was repeated using 30-min averaged observations, yielding a comparable value of $1.85\,\mathrm{m}$. The small difference between the 5- and 30-min estimates ($\sim 1.1\%$) indicates that the inferred effective aerodynamic roughness length is relatively insensitive to the averaging period considered. Given the small spatial variability in z_0 over the simulated LES domain (Figure 1c), both estimates support the use of $z_0 = 1.9\,\mathrm{m}$, which was applied uniformly throughout the LES domain.

To assess the robustness of this estimate, z_0 was also calculated using wind speed observations from towers measuring at 30 m above ground level. These measurements are located above the canopy top and therefore closer to the constant-flux layer where the assumptions of MOST are better satisfied. Although only five towers provide complete measurements at this height, the resulting z_0 (≈ 1.8–$1.9\,\mathrm{m}$) are consistent with those derived from the 10 m observations. This agreement supports the use of $Z_0 = 1.9\,\mathrm{m}$ as a representative effective aerodynamic roughness for the forested terrain of the Perdigão site. The observation-derived z_0 represents the surface conditions influencing the tower measurements and is not intended to characterize the roughness of an individual 30-m grid cell. In the present LES configuration, individual canopy elements

https://doi.org/10.5194/wes-2026-216
Preprint. Discussion started: 26 November 2026
© Author(s) 2026. CC BY 4.0 License.



eawe european academy of wind energy
Open Access WIND ENERGY SCIENCE DISCUSSIONS

are not explicitly resolved; therefore, z_0 accounts for their unresolved influence on surface momentum exchange within the surface-layer formulation.

An important distinction between the observational retrieval and the WRF surface-layer formulation is the treatment of (d). In the observational calculations, d is included to account for the displacement of the mean wind profile by the forest canopy, whereas the revised MM5 surface-layer scheme used in WRF does not explicitly account for d. To assess the sensitivity of the estimated z_0 to this assumption, we repeated the calculations using the same observations but setting $d = 0$. The resulting z_0 is approximately 2.2 m, compared with the prescribed value of 1.9 m obtained when d is considered. Although this difference introduces uncertainty in the correspondence between the observational estimate and the model parameter, both values are substantially larger than the default z_0 of approximately 0.1 m. Furthermore, the application of classical MOST over complex terrain introduces additional uncertainty because its underlying assumptions may not be fully satisfied under heterogeneous terrain and flow conditions.

After estimating z_0 (1.9 m), we hypothesize that this higher z_0 value, characteristic of a forest canopy, should be accompanied by adjustments of other land surface properties. A $Z_0 = 1.9\,\mathrm{m}$ typically corresponds to tall vegetation such as a forest of ≈ 13–$19\,\mathrm{m}$ tall trees (based on $Z_0/h = 0.1$–0.15). This implies that additional biophysical parameters such as albedo, emissivity, and LAI must also be reconsidered, as they are interrelated and strongly dependent on the vegetation type. For example, forests generally exhibit lower albedo compared to grasslands or shrublands, due to their reduced ability to reflect incoming solar radiation, which results in greater solar energy absorption.

Based on this analysis, we find that the land use categories assigned to the Perdigão area according to the CORINE database (i.e., *Mixed Shrubland/Grassland* and *Cropland/ Woodland Mosaic*) do not accurately represent the actual surface cover. Figure 1d shows the average z_0 in the CORINE database used in the LES domain over Perdigão valley is about 0.1 m. The Perdigão domain is dominated by *pine* and *eucalyptus* trees (Menke et al., 2019; Wise et al., 2022; Al Oqaily et al., 2025), which are both considered *evergreen forest* species. Therefore, we implement two key changes in our WRF-LES setup for MOD: (1) we reclassified the land use category over the Perdigão domain from *Mixed Shrubland/Grassland* to *Evergreen Needleleaf Forest*, and (2) we explicitly assign a z_0 value of 1.9 m to better represent the aerodynamic characteristics of the existing forest canopy. In WRF, several surface biophysical parameters—including albedo, emissivity, and LAI are prescribed according to the land-use category through the vegetation parameter look-up table (VEGPARM.TBL). Consequently, after the land-use reclassification these parameters are automatically updated to the values associated with the Evergreen Needleleaf Forest category in the CORINE-based table. The resulting differences in these biophysical parameters between the simulations are described in Section 2.3.

2.2.2 Surface Energy Budget

z_0 influences the dynamics of the surface boundary layer, including momentum flux as well as H and LE (Kadivar et al., 2021; June et al., 2018), by significantly altering the exchange processes between the land surface and the atmosphere. This, in turn, enhances heat transfer near the surface and impacts the surface energy budget. We thus decompose the energy budget as follows to analyze the impact of changes in z_0, and different vegetation structures, specifically albedo and LAI:

https://doi.org/10.5194/wes-2026-216
Preprint. Discussion started: 26 November 2026
© Author(s) 2026. CC BY 4.0 License.



eawe european academy of wind energy
Open Access WIND ENERGY SCIENCE DISCUSSIONS

$$SW_{\text{net}} = (1-\alpha)\cdot SW_{\downarrow} \tag{5}$$

$$LW_{\uparrow} = \sigma \cdot TSK^4 \tag{6}$$

$$LW_{\text{net}} = \varepsilon \cdot (LW_{\downarrow} - LW_{\uparrow}) \tag{7}$$

$$R_{\text{net}} = SW_{\text{net}} + LW_{\text{net}} \tag{8}$$

$$R_{\text{net}} = H + LE + G \tag{9}$$

where R_{net} is the net radiative flux at the surface (W m^{-2}), α is the albedo (dimensionless), representing the fraction of solar radiation reflected by the surface. $SW_{\downarrow}$ is the incoming shortwave radiation flux (W m^{-2}). σ is the Stefan–Boltzmann constant, TSK is the surface skin temperature (K), and ε is the emissivity (dimensionless). $LW_{\downarrow}$ and $LW_{\uparrow}$ are the downward and upward longwave radiation fluxes, respectively (W m^{-2}). G is the ground heat flux (W m^{-2}), and H and LE are expressed in W m^{-2}.

2.2.3 Turbulence Diagnostics

In this study, we also characterize the turbulence structure and its sensitivity to the surface modifications using turbulent kinetic energy (TKE), component-wise velocity variances, and vertical Reynolds stresses.

The resolved velocity variances $\overline{u'^2}$, $\overline{v'^2}$, and $\overline{w'^2}$ quantify the magnitude of the turbulent fluctuations in the three velocity components. To characterize turbulent momentum transport, we additionally calculate the resolved vertical Reynolds stresses $\overline{u'w'}$ and $\overline{v'w'}$, which represent the covariance between the horizontal and vertical velocity fluctuations and provide information on the vertical turbulent transport of horizontal momentum.

For the vertical-profile analysis, the resolved velocity variances and Reynolds stresses are first calculated at each horizontal grid-cell center and model vertical level using the selected one-hour averaging period. The temporal mean velocity at each grid point is used to define the velocity fluctuations, from which $\overline{u'^2}$, $\overline{v'^2}$, $\overline{w'^2}$, $\overline{u'w'}$, and $\overline{v'w'}$ are calculated. For each horizontal grid column along the cross-section, the geometric height of each model level is expressed relative to the local terrain elevation to obtain height above ground level (AGL). Because the terrain-following model levels occur at different AGL heights across the complex terrain, each vertical profile is interpolated onto a common AGL grid with 10-m vertical spacing from 0 to 500 m. The interpolated profiles are then horizontally averaged over three representative regions along the cross-section corresponding to the windward slope, valley, and downwind slope.

In addition, turbulent kinetic energy (TKE) is calculated as:

$$\text{TKE} = \frac{1}{2}\left(\overline{u'^2} + \overline{v'^2} + \overline{w'^2}\right). \tag{10}$$

For the TKE analysis, velocity fluctuations are computed independently at each horizontal grid point and model vertical level over 5-minute periods, from which TKE is calculated at each model level and subsequently averaged over 15-minute intervals.

https://doi.org/10.5194/wes-2026-216
Preprint. Discussion started: 26 November 2026
© Author(s) 2026. CC BY 4.0 License.



eawe european academy of wind energy
Open Access WIND ENERGY SCIENCE DISCUSSIONS

To further evaluate the simulated turbulence statistics against observations, we analyze three ISFS towers (tse04, tse09, and tse13) located at the south ridge, valley, and ridge of the Perdigão site. These towers are also included in the evaluation of vertical wind speed profiles and provide measurements at common heights of 30, 40, 60, 80, and 100 m AGL.

The along-wind velocity variance, denoted by $\overline{u'^2_{\parallel}}$, where the subscript $\parallel$ indicates the direction parallel to the hourly mean horizontal wind, is calculated by projecting the horizontal velocity fluctuations onto this direction:

$$\overline{u'^2_{\parallel}} = \overline{\left(\frac{\overline{u}u' + \overline{v}v'}{\sqrt{\overline{u}^2 + \overline{v}^2}} \right)^2}. \tag{11}$$

The vertical velocity variance ($\overline{w'^2}$) and TKE are calculated following the definitions introduced above, but using velocity fluctuations relative to their hourly means. Given the temporal resolution of the available wind velocity records, these diagnostics do not capture high-frequency turbulent fluctuations and are therefore interpreted as proxies for turbulence statistics.

The hourly diagnostics are matched between observations, CTRL, and MOD, and subsequently averaged over the four-day study period to obtain vertical profiles at each tower. The standard deviation of the hourly diagnostics is used to quantify their temporal variability.

2.3 WRF-LES Model Configuration

In this study, four multiscale numerical simulations are performed with the WRF model v4.4 (Skamarock et al., 2019) and its LES component to test the sensitivity of atmospheric properties to land-surface properties. Accurate high-resolution wind modeling requires a multiscale modeling framework, in which mesoscale weather models (with grid spacing $\Delta x \geq 1$ km) provide boundary and initial conditions for microscale flow models (Δx on the order of tens of meters) through a series of nested domains. This meso–micro coupling approach has been widely used in recent studies to capture interactions between large-scale atmospheric forcing and local-scale turbulence and surface processes (e.g., Giani et al. (2022); De Moliner et al. (2024); Giani and Crippa (2024); Janiszeski and Crippa (2025); Al Oqaily et al. (2025)). Specifically, we adopt a five nested-domain configuration spanning the mesoscale (d01–d02), the gray zone (d03–d04), and the microscale (d05, configured in LES mode), with horizontal grid spacings of 11.25 km (d01), 3.75 km (d02), 750 m (d03), 150 m (d04), and 30 m (d05) (Figure 1), similar to (Al Oqaily et al., 2025).

The WRF model is a fully compressible and non-hydrostatic model that solves the Euler equations in hybrid coordinates. This model offers multiple options for each physical process. The chosen physics packages include the unified Noah land surface scheme (Ek et al., 2003), the Rapid Radiative Transfer Model for General Circulation Models (RRTMG) for longwave radiation (Mlawer et al., 1997), and the Dudhia scheme for shortwave radiation (Dudhia, 1989). The revised MM5 surface layer scheme (Jiménez et al., 2012) is also used. The Kain–Fritsch cumulus scheme (Kain and Fritsch, 1990) is applied only in the outer domain (d01) with $\Delta x \approx 11.25\,\text{km}$.

Four simulations are conducted to investigate the sensitivity of wind speed to vertical resolution and surface roughness representation (Figure 2). The baseline configuration (Control, CTRL) follows the same domain setup as the 36 simulations in (Giani and Crippa, 2024) and adopts the physics configuration identified as optimal in (Al Oqaily et al., 2025). In addition

https://doi.org/10.5194/wes-2026-216
Preprint. Discussion started: 26 November 2026
© Author(s) 2026. CC BY 4.0 License.

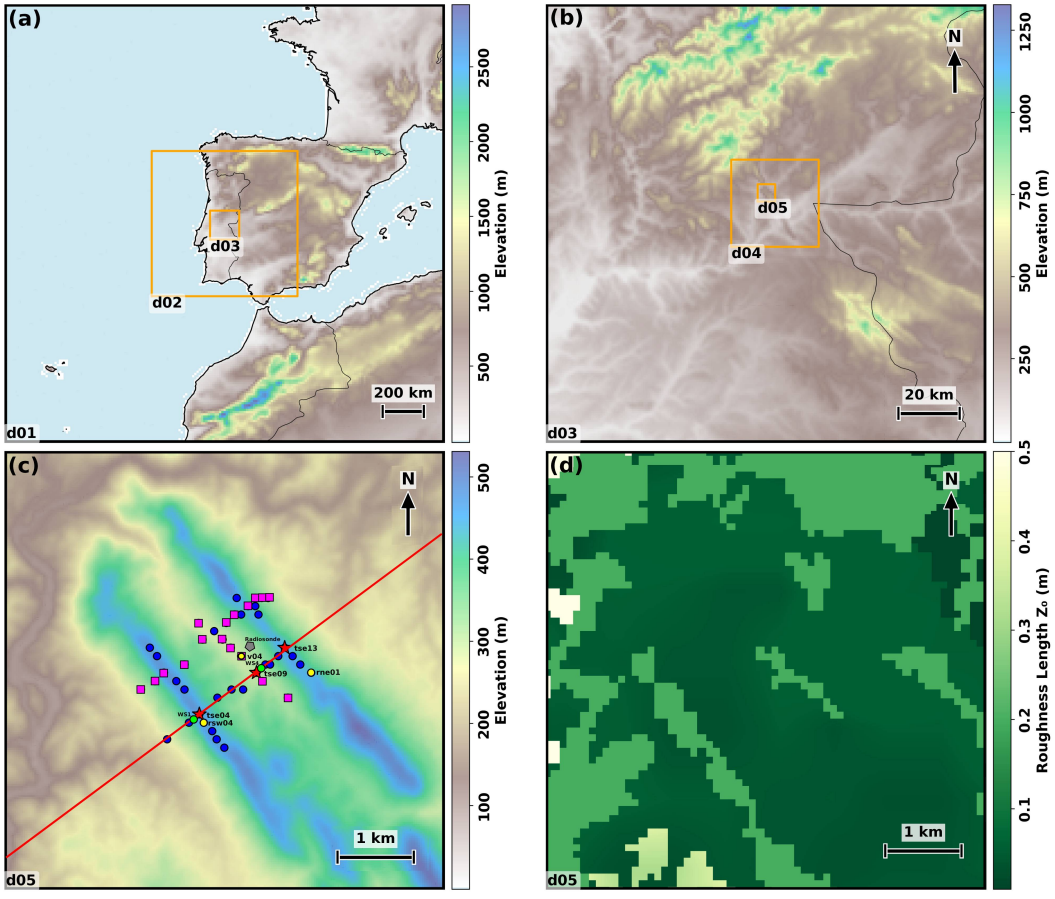


Figure 1. Five nested-domain configuration (d01–d05) for the multiscale WRF simulations. Panels (a)–(b) show the model domains with terrain elevation from the U.S. Geological Survey (USGS). Panel (c) displays the d05 domain (LES resolution) elevation from the Shuttle Radar Topography Mission (SRTM), while panel (d) presents the z_0 in the CORINE Land Cover dataset used in d05. Dots and squares indicate the locations of ISFS towers along the ridge, valley, and transect analyzed in this study. Pink squares mark towers used to estimate z_0, red stars indicate towers with wind speed measurements at multiple heights, and yellow dots represent towers with surface radiation measurements. All towers, including those marked with blue dots, are used to evaluate the simulations. The DTU Doppler wind lidars WS1 and WS4 are labeled with green dots; WS2 and WS3 are located close to WS1 and WS4 and are therefore not shown. The gray pentagon marks the location of radiosonde data. The red line in (c) denotes the transect along which cross-section analyses are performed.

to CTRL, three sensitivity simulations are conducted to investigate the impact of vertical resolution and surface properties representation (Figure 2). The simulation CTRL-N_z modifies only the vertical grid configuration by reducing the number of vertical levels from $N_z = 109$ to $N_z = 75$, while keeping the land-surface properties identical to CTRL. This allows us to isolate the impact of vertical resolution on wind speed simulations. The simulation CTRL-z_0-N_z combines the coarser vertical grid spacing with an increased aerodynamic roughness length ($Z_0 = 1.9$ m) while maintaining the same land-use category and

https://doi.org/10.5194/wes-2026-216
Preprint. Discussion started: 26 November 2026
© Author(s) 2026. CC BY 4.0 License.



eawe european academy of wind energy
Open Access WIND ENERGY SCIENCE DISCUSSIONS

associated surface parameters (e.g., albedo and LAI) as CTRL, which are derived from the CORINE dataset. This configuration allows us to isolate the effect of z_0 on the simulated wind fields without modifying other land-surface properties. Finally, the modified simulation (MOD) adopts the increased z_0, a different land-use category for the Perdigão area (evergreen needleleaf forest), and the coarser vertical grid configuration (N_z = 75). This setup is considered more physically consistent, since z_0 of 1.9 m is not representative of grassland surfaces and is instead associated with tall vegetation such as forests. Therefore, MOD provides a more realistic land-surface characterization by jointly adjusting key surface parameters—including z_0, $albedo$, and LAI—to reflect the Perdigão site conditions, as described in Section 2.2.

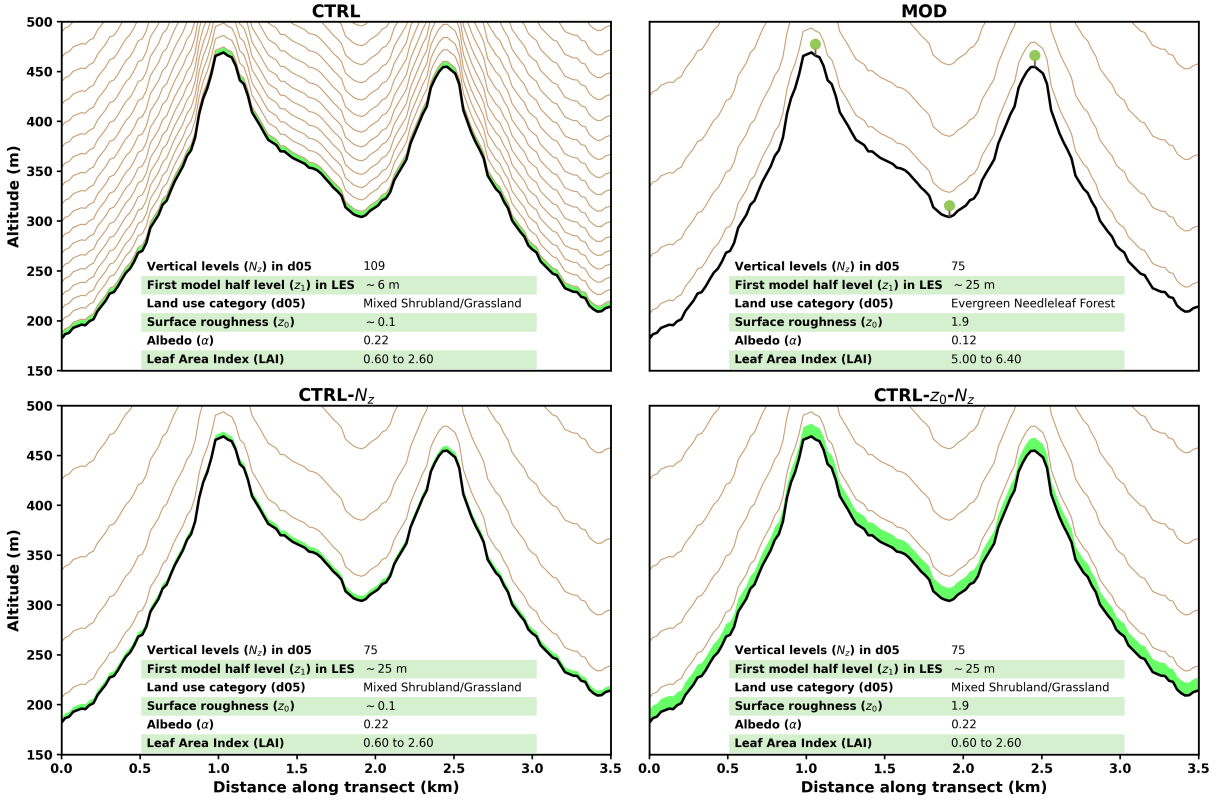


Figure 2. Schematic representation of the four numerical experiments used in this study. The panels illustrate the vertical grid configuration and land-surface properties for each simulation: CTRL (top-left), MOD (top-right), CTRL-N_z (bottom-left), and CTRL-z_0-N_z (bottom-right). The experiments are designed to isolate the effects of vertical resolution and z_0, and to distinguish these from changes in other land-surface parameters introduced by modifying the land-use category. The light green shaded area represents the vegetation layer near the surface (grassland) with different value of z_0, while the trees (top-right) represent the forest, illustrating its position relative to the first model half level.

The vertical resolution for CTRL ranges from 77 levels in d01–d03 to 91 and 109 levels in d04 and d05, respectively. The first model half level, where horizontal velocities, pressure, and scalars are calculated, is $z_1 \approx 6$ m in the LES domain (d05), placing it below the height of the dominant forest canopy. The corresponding near-surface grid aspect ratio ($\Delta x/\Delta z$)

https://doi.org/10.5194/wes-2026-216
Preprint. Discussion started: 26 November 2026
© Author(s) 2026. CC BY 4.0 License.



eawe european academy of wind energy
Open Access WIND ENERGY SCIENCE DISCUSSIONS

is approximately 2.5 ($\Delta x = 30$ m, $\Delta z \approx 12$ m). For the simulations CTRL-N_z, CTRL-z_0-N_z, and MOD, 75 vertical levels are used in all domains. The eta levels are configured with increasing Δz, starting from $\Delta z_s = 50$ m near the surface and reaching an approximately constant $\Delta z_f = 270$ m in the free atmosphere. The selected configuration places the first model half level at $z_1 \approx 25$ m, above the canopy (Figure 2, top-right), and results in a near-surface grid aspect ratio of approximately 0.6 ($\Delta x = 30$ m, $\Delta z \approx 50$ m). As part of the grid-selection process, sensitivity tests were conducted with the lowest model level located both within and above the canopy, and with an alternative above-canopy configuration having a near-surface aspect ratio of approximately 1.1. These tests produced very similar wind statistics and did not alter the main conclusions of the study (Figure S2), indicating that the simulated flow is relatively insensitive to moderate changes in vertical-grid placement and aspect ratio. We acknowledge that the optimal aspect ratio in terrain-following LES simulations remains an active area of research. While aspect ratios substantially larger than unity are often recommended in idealized studies (Wyngaard et al., 1998), previous studies have emphasized that recommendations derived from idealized flat-terrain simulations may not be directly applicable to simulations over complex terrain, where terrain-following coordinates can introduce additional truncation errors in horizontal derivative calculations and grid-cell skewness over steep terrain (Mirocha et al., 2010; Mahrer, 1984). Previous WRF-LES studies generally recommend aspect ratios of order unity rather than identifying a sharp threshold at exactly one (Liu et al., 2020; Giani et al., 2022), and sensitivity studies indicate that aspect-ratio effects tend to occur gradually and are most pronounced for substantially larger aspect ratios (Nishizawa et al., 2015; Daniels et al., 2016). Therefore, the suitability of the adopted aspect ratio is assessed here based on direct sensitivity testing, which provides a case-specific evaluation of its influence on the simulated near-surface winds over complex terrain. The adopted configuration was therefore retained because it keeps the lowest model level above the canopy and roughness sublayer, providing a more physically consistent coupling between the surface-layer parameterization and the resolved flow above the canopy. This configuration should not be interpreted as resolving canopy-scale turbulence more realistically. Rather, because the present WRF setup does not include an explicit canopy-drag parameterization, placing the first model level above the canopy avoids locating the lowest model level within the canopy and roughness sublayer, where the assumptions of MOST are less applicable (Harman and Finnigan, 2007). The resulting simulations are therefore intended to provide a more physically consistent coupling between the surface-layer parameterization and the resolved flow above the canopy, rather than an explicit representation of in-canopy turbulence.

z_0 and land-use modifications were applied exclusively within the innermost LES domain (d05). All simulations employ one-way nesting, so these modifications do not affect the parent domains. CTRL-N_z, CTRL-z_0-N_z, and MOD share identical configurations in the gray-zone domains (d03–d04), including their vertical grids and land-surface properties, and therefore receive identical lateral boundary forcing in d05. In contrast, CTRL uses a different vertical-grid configuration in the parent domains, which may influence the meteorological conditions entering d05.

All simulations share the following settings, which are chosen based on the best physical and statistical evaluation (Al Oqaily et al., 2025). Initial and lateral boundary conditions are driven every hour by the fifth-generation ECMWF atmospheric reanalysis (ERA5), which has a grid resolution of $\Delta x = 0.25°$ and is updated hourly (Hersbach et al., 2020). The topography and land use data are specified based on NASA's Shuttle Radar Topography Mission (30 m resolution) and the Coordination of Information on the Environment (CORINE) land use data (100 m resolution), respectively. The Shin–Hong (Shin and Hong, 2015)

https://doi.org/10.5194/wes-2026-216
Preprint. Discussion started: 26 November 2026
© Author(s) 2026. CC BY 4.0 License.



eawe european academy of wind energy
Open Access WIND ENERGY SCIENCE DISCUSSIONS

turbulence closure in the gray zone domains (d03 and d04) is applied to compute subgrid turbulent fluxes of heat, moisture, and momentum. Although Shin–Hong was originally developed and evaluated primarily for vertical sensible heat transport in idealized dry convective boundary layers, its application to moisture and momentum transport relies on similarity assumptions between heat, scalar, and momentum transport. These assumptions may introduce uncertainty in the representation of subgrid moisture and momentum fluxes, particularly under stable nighttime, strong vertical wind shear, and transitional atmospheric conditions relevant to the present study. Finally, the Turbulent Kinetic Energy (TKE) closure of Deardorff (Deardorff, 1980) is used for the subgrid-scale (SGS) model in the LES domain (d05). The entire set of the model configurations, selected physics parameterizations, and differences between the simulations are listed in Table S1. The simulation period is run for four consecutive days from May 19 00UTC to 23 May 00 UTC for the four simulations.

2.4 Model Evaluation Metrics

Model performance is evaluated using statistical metrics including the root-mean-square error (RMSE), mean bias (MB), and correlation coefficients (R), computed by comparing simulated and observed ISFS wind speed at tower locations.

RMSE is evaluated using multiple aggregation approaches. For spatial analysis, values are averaged across all available towers at each time step and then aggregated over the selected period. For temporal analysis, RMSE is computed at each tower by averaging over time. For towers with vertical profile measurements (tse04, tse09, and tse13), RMSE is also calculated at each vertical level and averaged over the analysis periods. MB is calculated as the difference between simulated and observed values (WRF - ISFS). All metrics are evaluated separately for the defined periods (e.g., daytime, nighttime, and transition periods) to assess sensitivity to atmospheric stability and modeling configurations.

3 Results

3.1 Temporal and Spatial Surface Wind Speed Response to Enhanced z_0

In this section, we first analyze the temporal evolution of spatially averaged wind speed to assess how these changes develop over time. We then evaluate the spatial distribution of surface wind speed to identify localized patterns associated with the enhanced z_0 changes. We begin by analyzing the high-frequency temporal variability using the 5-minute simulated output. Figure 3 shows the time series of 5-minute averaged U10 across all ISFS towers for the LES simulations with different model configurations and the observed values. Four simulations are compared: the baseline configuration (CTRL), the simulation with reduced vertical levels (CTRL-N_z), the simulation including both vertical levels and modified surface roughness (CTRL-z_0-N_z), and the modified land-use configuration (MOD).

The CTRL simulation systematically overestimates near-surface wind speed across all tower groups. Reducing the number of vertical levels (CTRL-N_z) partially reduces this bias, indicating that simply using a finer vertical resolution does not necessarily reduce near-surface wind speed biases in LES configurations. We speculate that the improved agreement with observations obtained when the first model level is located at approximately 25 m is primarily associated with a more appropriate

https://doi.org/10.5194/wes-2026-216
Preprint. Discussion started: 26 November 2026
© Author(s) 2026. CC BY 4.0 License.

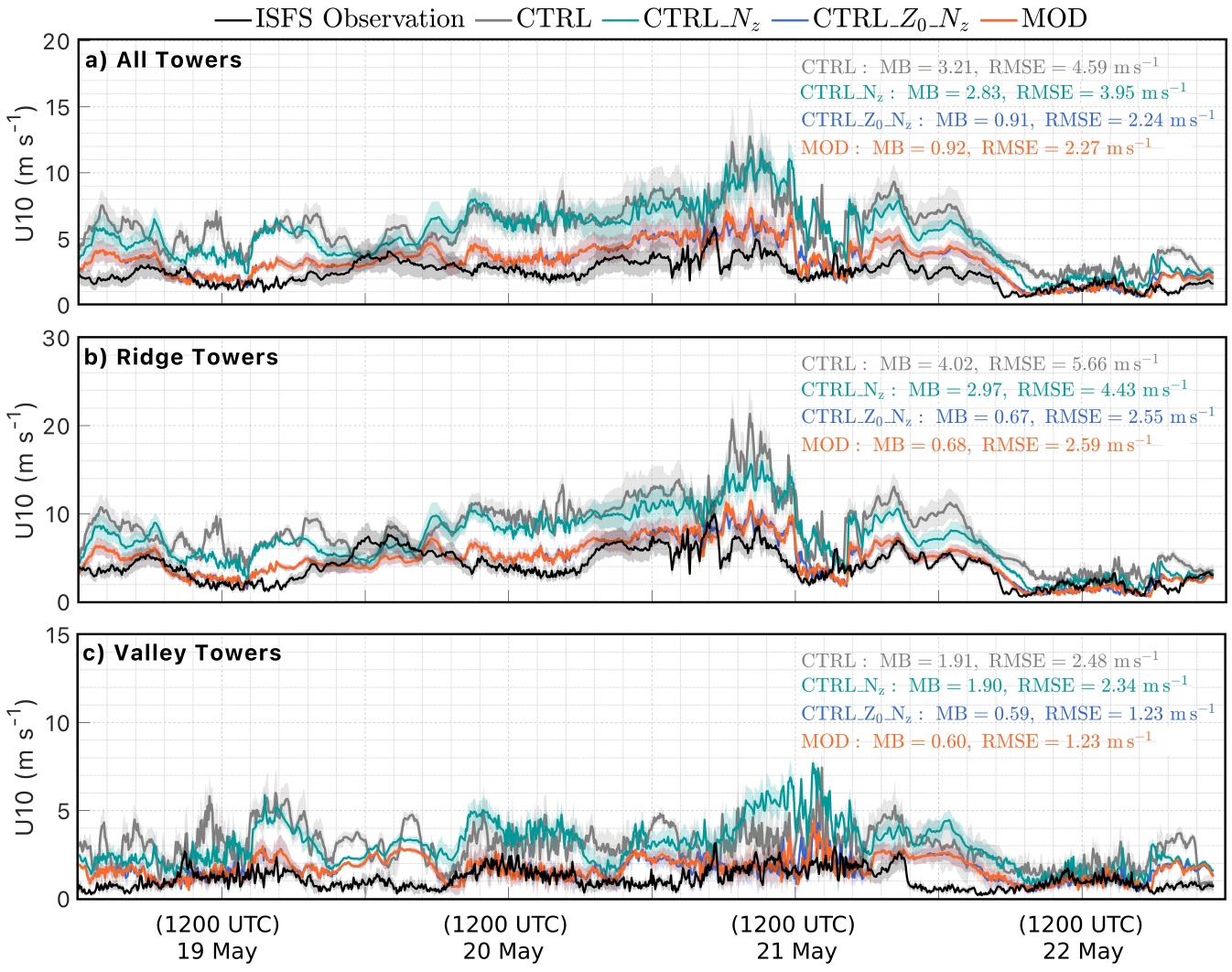


Figure 3. Time series of U10 (m s^{-1}) for ISFS observations and WRF simulations in the LES domain (d05), averaged over different tower groups during the Perdigão experiment. Panels show averages across (a) all ISFS flux towers, (b) ridge towers, and (c) valley towers. The black line represents ISFS observations. Model simulations include the baseline configuration (CTRL, grey), the simulation with reduced vertical levels (CTRL-N_z, green), the simulation with reduced vertical levels and modified surface roughness (CTRL-z_0-N_z, blue), and the modified land-use configuration (MOD, orange). Shaded areas indicate the spread among ISFS towers within each group.

representation of the near-surface flow. In the CTRL configuration, the first model level is located within the canopy, where the assumptions underlying the MOST theory are no longer valid. Placing the first model level above the canopy provides a more appropriate application of the surface-layer parameterization and may also influence the representation of near-surface shear

https://doi.org/10.5194/wes-2026-216
Preprint. Discussion started: 26 November 2026
© Author(s) 2026. CC BY 4.0 License.



eawe european academy of wind energy
Open Access WIND ENERGY SCIENCE DISCUSSIONS

and the balance between resolved and subgrid-scale turbulence, consistent with previous studies Khanna and Brasseur (1997); Maronga (2014); Arthur et al. (2019).

A much larger improvement is observed when z_0 is increased (CTRL-z_0-N_z), which substantially improves agreement with observations. This comparison, between CTRL-N_z and CTRL-z_0-N_z, isolates the effect of increasing z_0 because the vertical grid and land-use category are unchanged between the two simulations. In contrast, modifying the land-use category (MOD) produces only a small additional improvement relative to CTRL-z_0-N_z.

The incremental experiments allow us to quantify the relative contribution of each modeling choice. For all towers, reducing the number of vertical levels reduces the RMSE by approximately 0.64 m s^{-1}, corresponding to about 27% of the total improvement relative to CTRL. Increasing z_0 produces the largest improvement, reducing the RMSE by approximately 1.71 m s^{-1}, corresponding to roughly 73% of the total error reduction. In contrast, modifying the land-use category results in only a minor additional improvement in wind speed. Importantly, the improvement associated with increased z_0 occurs despite the coarser near-surface vertical resolution, further highlighting the primary role of canopy drag in controlling the boundary-layer flow over the forested terrain.

This pattern is consistent across terrain types. For ridge towers, both vertical resolution and z_0 contribute to the improvement, although the effect of z_0 remains dominant. In valley locations, the improvement is almost entirely explained by the increase in z_0, while vertical resolution plays only a minor role.

These results indicate that z_0 is the primary factor controlling the improvement of simulated near-surface winds. In particular, the comparison between CTRL-N_z and CTRL-z_0-N_z, which differ only in z_0 , demonstrates that most of the reduction in wind-speed bias is achieved by increasing z_0. The land-use category modification itself has only a secondary effect on wind speed once z_0 is correctly represented. Therefore, in the remainder of this study, we focus primarily on the comparison between the CTRL and MOD simulations. The CTRL simulation is retained as the reference configuration to facilitate comparison with our previous studies Giani and Crippa (2024); Al Oqaily et al. (2025), whereas MOD represents the most physically realistic configuration for the Perdigão site. This focus does not imply that the attribution to z_0 is based solely on the CTRL–MOD comparison; rather, the attribution is supported by the incremental sensitivity experiments discussed above. Furthermore, prescribing $Z_0 = 1.9$ m while retaining the default grassland/shrubland land-use category is useful as an isolation experiment, but it is not physically consistent with the observed pine and eucalyptus forest cover, which differs substantially in vegetation structure, albedo, LAI, all of which influence land–atmosphere exchanges.

Overall, the RMSE decreases from 4.59 m s^{-1} in CTRL to approximately 2.27 m s^{-1} in MOD, indicating a reduction of more than 50% in RMSE due to the implemented changes at LES resolution throughout the simulation period. These findings highlight the critical role of land-use datasets in determining the accuracy of numerical simulations, particularly for near-surface variables. While LES offers fine-scale insights, higher resolution alone does not guarantee better accuracy, especially in complex mountainous terrain. Proper land-surface representation is therefore crucial: combining high-resolution topography with accurate land use is essential, since incorrect z_0 values can systematically bias the wind speed and flow.

https://doi.org/10.5194/wes-2026-216
Preprint. Discussion started: 26 November 2026
© Author(s) 2026. CC BY 4.0 License.



eawe european academy of wind energy
Open Access WIND ENERGY SCIENCE DISCUSSIONS

Building on the focus on the CTRL and MOD simulations, we next examine the spatial distribution of surface wind speed to identify localized patterns and variability associated with enhanced z_0. Specifically, we discuss the impact of z_0 on instantaneous U10 from two days characterized by contrasting inflows to the LES domain (d05, Δx = 30 m).

Analyses of May 20 at 1200 UTC show northeasterly flow in both runs (Figure 4, first row), while on May 21 at 2200 UTC, the wind reverses and blows from the southwest, shifting the direction of flow (Figure 4, second row). For both events, CTRL exhibits higher U10, whereas MOD leads to a marked reduction in surface winds (Figure 4). In CTRL, U10 appears overestimated, particularly within the valley, over the ridge tops, and on the lee side of the downwind ridge, as indicated by the larger RMSE values at the ISFS tower locations. However, in MOD, after increasing z_0 and updating the land use, the wind flow is reduced within the valley, downstream of complex terrain, and above the ridge tops.

This reduction in wind speed in MOD is consistent with the enhanced surface drag associated with the increased z_0. The unrealistically high wind speeds in CTRL are likely due to the underestimated z_0 associated with the incorrect land use classification in the CORINE dataset. These findings are also supported by previous evaluations of WRF-LES runs over the Perdigão site, which showed that high-resolution simulations tend to exhibit larger wind speed biases if not properly configured (Al Oqaily et al., 2025; Wagner et al., 2019b).

Flow variability in complex terrain exhibits significant spatial differences, as local topography, elevation, and land surface characteristics strongly influence wind speed at different locations. Figures 3b and 3c show the time series of U10 averaged across ridge and valley towers for both runs, respectively. To assess the model's ability to capture spatial flow dynamics at LES resolution, which better resolves complex terrain, we examine differences in z_0 and model performance. As described in Section 2.2, both ridge and valley tower locations have similar estimated z_0 of approximately 1.9 m, primarily due to the widespread presence of tall trees throughout the Perdigão domain. However, the impact of increasing z_0 is more pronounced at ridge locations. Figure S3 clearly shows that the RMSE drops significantly at ridge towers in MOD compared to CTRL, with reductions of up to 4.5 m s^{-1}. In contrast, most valley towers exhibit less than a 1 m s^{-1} change in RMSE. This difference can be attributed to stronger wind speeds typically observed over mountaintops, which is related to the different flow accelerations driven by the different pressure fields that develops around the topography. We find that the greater overestimation in CTRL over the ridges, associated with an insufficient representation of z_0, coincides with higher wind speeds relative to valley locations, which generally exhibit lower wind speeds due to stable boundary layer conditions and topographic sheltering effects (Al Oqaily et al., 2025).

To further evaluate how the modified surface representation influences U10, we quantify the correlation in U_{10} between the CTRL and MOD simulations. This comparison helps determine whether the impact of Z_0 can be represented as a simple bias or involves more complex flow adjustments that cannot be corrected post-simulation. Figure S4 compares U_{10} across all towers, ridge towers, and valley towers. Overall, the two simulations are strongly correlated ($R = 0.89$), suggesting that the large-scale response to increased z_0 can be largely represented as a systematic reduction in wind speed. The relationship remains robust over ridge towers ($R = 0.87$), where MOD behaves as a bias-correctable version of CTRL. In contrast, valley towers show a much weaker correlation ($R = 0.34$) and a flatter slope, indicating that enhanced z_0 induces localized and nonlinear flow responses that cannot be captured by a simple linear correction of CTRL. This raises an important question explored in the

https://doi.org/10.5194/wes-2026-216
Preprint. Discussion started: 26 November 2026
© Author(s) 2026. CC BY 4.0 License.

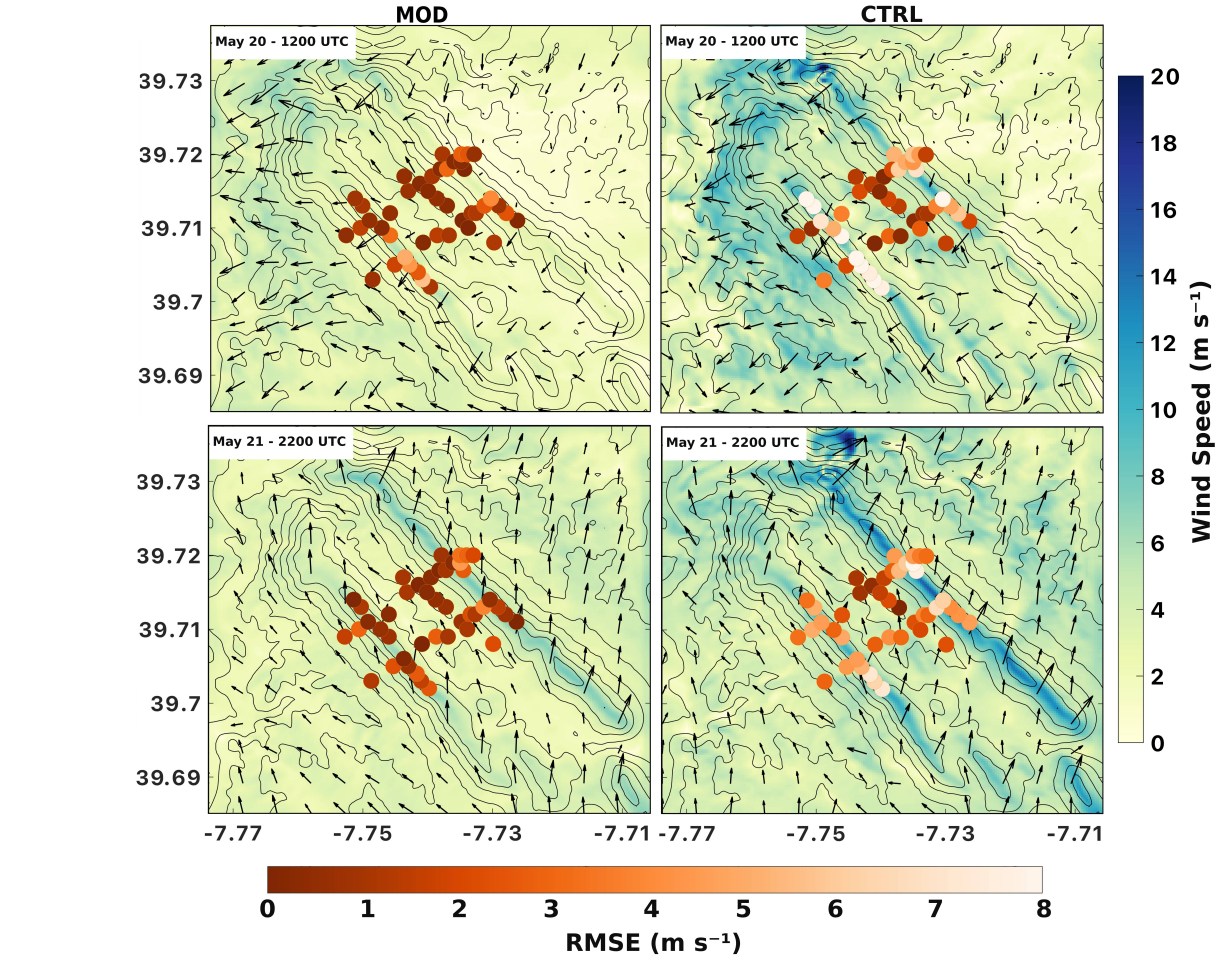


Figure 4. Example of instantaneous U10 (shading, m s^{-1}) and direction (black arrows) for CTRL (right) and MOD (left) at 1200 UTC on 20 May and 2200 UTC on 21 May over the LES (d05) resolution. Terrain height is represented by black contours with a spacing of 50 m, 300 m in the valley, and 450 m at the top ridge. Colored dots (orange) indicate the RMSE between the WRF simulations and ISFS observations at each tower location.

following sections: does modifying Z_0 simply reduce wind magnitudes, or does it fundamentally alter wind patterns and flow structures, especially within complex terrain?

3.2 z_0 Influence on Intra-daily Variability and Vertical Structure of Wind Profiles

In this section, we analyze how changes in z_0 affect the vertical wind speed profile during different atmospheric conditions. We focus on three key sub-periods: (i) daytime convective conditions (12–15 UTC), (ii) nighttime stable conditions (00–03 UTC,

https://doi.org/10.5194/wes-2026-216
Preprint. Discussion started: 26 November 2026
© Author(s) 2026. CC BY 4.0 License.



eawe european academy of wind energy
Open Access WIND ENERGY SCIENCE DISCUSSIONS

May 19–21), and (iii) a synoptic transition (12 UTC May 21 – 06 UTC May 22), when a significant wind shift occurs, as also analyzed in De Moliner et al. (2024); Al Oqaily et al. (2025). The vertical profiles are evaluated using RMSE between both model runs and ISFS observations at multiple sensor altitudes across three towers (tse04, tse09, tse13). Additionally, cross-sectional analyses of wind speed at selected instants are presented to illustrate how wind flow patterns respond to different land surface characteristics.

Vertical wind profiles for both runs and ISFS observations are shown in Figure 5a–d from 10 m to the maximum ISFS observation level available (100 m), and are averaged across different time periods over three flux towers. Overall, the shape of MOD wind profiles and ISFS observations are generally consistent with previous studies (Harman and Finnigan, 2007; Hung et al., 2024; Bonan et al., 2018). MOD wind profiles all show a similar pattern with a logarithmic profile above the canopy, associated with the MOST effects, whereas CTRL does not follow that behavior, especially below 20 m. Moreover, the vertical wind speed profile of MOD increases more rapidly (i.e., $\frac{dU}{dz}$ is lower with elevation) in comparison with CTRL. This is also apparent in the observations and is due to the theoretical wind profile above the forest (North et al., 2014). Near the surface, vegetation drag slows the wind substantially. With increasing height, the effect of drag diminishes, and the wind accelerates until the surface influence is no longer felt (Szkordilisz and Zöld, 2016).

From Figure 5a and 5b, which show the daytime convective and nighttime stable periods, respectively, it is notable that there is a difference in the effect of z_0 changes below and above specific elevations. Within the surface layer, the effects of z_0 and friction are dominant in shaping the wind profiles. Surface drag effects (friction and z_0) dominate the surface layer, which constitutes the lowest $\sim$10% of the boundary layer, and is the region where MOST is most applicable and performs well (Stull, 2012; North et al., 2014). The height of the surface layer exhibits notable diurnal variability. During daytime, strong convective mixing can produce a mixed layer depth of approximately 1000 m, with the surface layer typically extending to $\sim$100 m. In contrast, under stable nighttime conditions—especially during clear, calm nights—the boundary layer may be only tens to a few hundred meters deep, particularly in valleys where its depth can be on the order of tens of meters. The surface layer can become as shallow as $\sim$10 m. This substantial reduction in depth limits the practical value of surface-layer-based approaches during the night. Thus, during stable nighttime conditions, the vertical wind profiles from both runs become largely unaffected by changes in z_0 above a certain height. This occurs because the surface layer is very shallow, and the atmosphere above it becomes decoupled from surface influences, thereby minimizing differences between the two simulations.

Figure 5e–h presents the evaluation of vertical wind profiles using RMSE across all periods. The results show that surface wind speed RMSE is reduced by more than 50% in MOD compared to CTRL across all periods. Additionally, the RMSE consistently decreases with height, indicating improved performance of MOD throughout the lower boundary layer. This improvement is attributed to stronger surface friction associated with the enhanced z_0. The influence of z_0 is strongest near the surface where wind shear is largest. Moreover, both simulations exhibit the lowest RMSE during daytime, followed by the synoptic transition period, while the highest RMSE is observed during nighttime stable conditions. This suggests that accurately capturing wind speed is more challenging at night, particularly near the surface and into the lower boundary layer, as also supported by previous studies (De Moliner et al., 2024; Al Oqaily et al., 2025). This behavior is consistent with previous studies showing that numerical models often exhibit larger wind speed errors under stable stratification due to difficulties in

https://doi.org/10.5194/wes-2026-216
Preprint. Discussion started: 26 November 2026
© Author(s) 2026. CC BY 4.0 License.

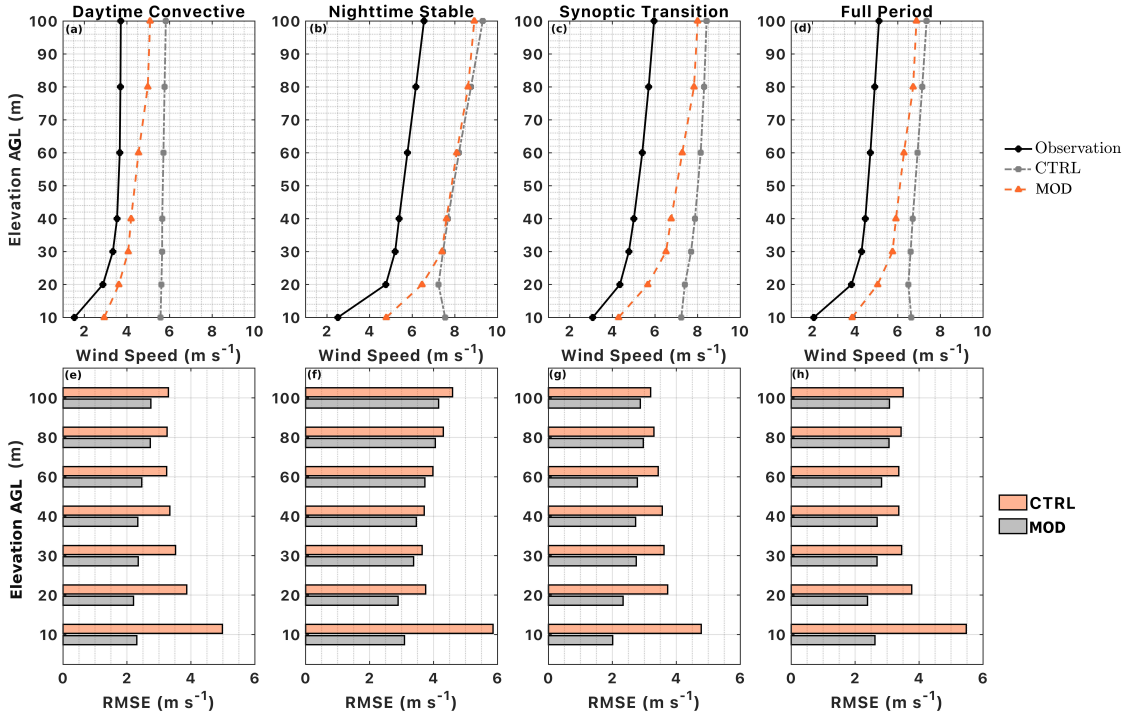
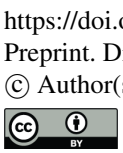


Figure 5. Vertical wind speed profiles (top row) and corresponding RMSE values (bottom row) at multiple sensor elevations (10–100 m) from ISFS observations and two model runs (CTRL and MOD) for four selected periods: (a, e) Convective (12–15 UTC), (b, f) Nighttime Stable (00–03 UTC, May 19–21), (c, g) Synoptic Transition (12 UTC May 21 – 06 UTC May 22), and (d, h) Full Period (00 May 19–00 May 23). Profiles and RMSE values are averaged over three flux towers (tse04, tse09, tse13).

representing weak and intermittent turbulence in the nocturnal boundary layer (Ngan et al., 2013). Under stable conditions, turbulence becomes weaker and the characteristic size of turbulent eddies decreases, increasing the reliance on SGS parameterizations and making the representation of near-surface shear and turbulent mixing more sensitive to model resolution and turbulence closures (Basu and Porté-Agel, 2006). As a result, LES simulations of stable boundary layers can be particularly sensitive to the choice of SGS turbulence models and grid resolution (Stoll and Porté-Agel, 2008).

A variety of flow phenomena—such as thermally driven circulations, downslope windstorms, and lee waves—occur over complex terrain but remain challenging to represent in numerical models (Storm et al., 2009; Menke et al., 2019; Janiszeski and Crippa, 2025). Among these, low-level jets (LLJs) are of particular interest due to their relevance for wind energy production and their influence on boundary-layer processes and aerosol transport (Banta et al., 2004; Wagner et al., 2019a). In the Perdigão experiment, LLJ events were frequently observed and investigated in prior studies, with most cases identified as thermally driven flows induced by the surrounding mountainous terrain under synoptically calm conditions (Wagner et al., 2019a). Here, we analyze one such LLJ event at 0400 UTC on 22 May 2017, based on available lidar observations, to assess the impact of changes in z_0 on the structure and occurrence of LLJs over the double ridge. Figure 6c shows composites from the four

https://doi.org/10.5194/wes-2026-216
Preprint. Discussion started: 26 November 2026
© Author(s) 2026. CC BY 4.0 License.



eawe european academy of wind energy
Open Access WIND ENERGY SCIENCE DISCUSSIONS

DTU wind scanners (WS1–WS4), displaying the cross-valley wind component across the double ridge, retrieved from radial velocities. Gravity waves form above and downstream (lee side) of the double ridge. The sounding indicates wind shear, with southwesterly winds over the ridge veering to northerlies around 1 km altitude.

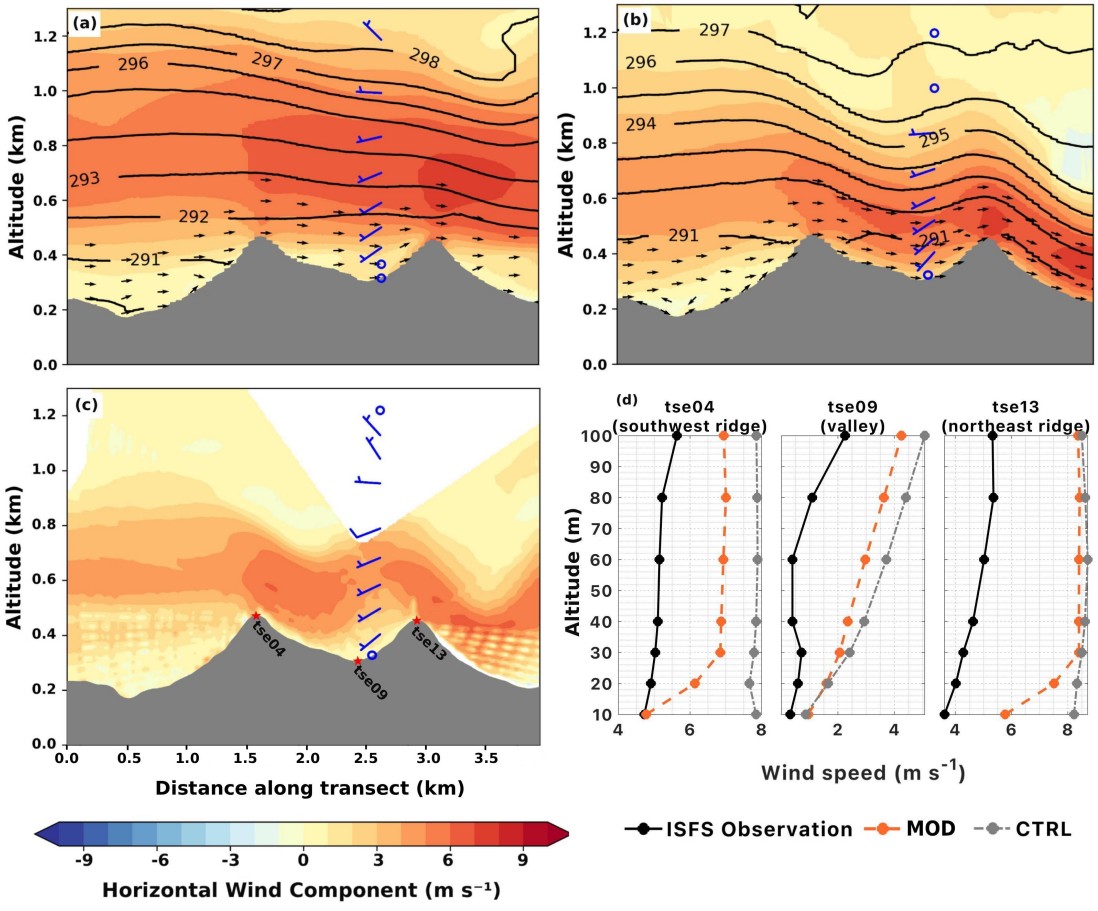


Figure 6. Cross sections and vertical profiles of cross-valley wind. Panels (a–c) show the horizontal wind component across the double ridge. (a) CTRL displays the simulated potential temperature (1 K contour intervals) with blue wind barbs indicating simulated horizontal wind speed and direction at the location of radiosondes launched in the valley. (b) MOD shows the corresponding simulation with increased z_0. (c) DTU lidar composite (WS1–WS4) depicts an observed low-level jet from the southwest on 22 May 2017 at 04:01:09 UTC, with the x-axis centered at WS1; negative velocities indicate flow from the northeast. Blue wind barbs correspond to horizontal wind speed and direction observed by radiosondes launched at 05 UTC (horizontal drift of the balloon is not considered). (d) Vertical profiles of wind speed at three towers—tse04 (southwest ridge), tse09 (valley), and tse13 (northeast ridge)—comparing ISFS observations (black), MOD (orange), and CTRL (gray).

https://doi.org/10.5194/wes-2026-216
Preprint. Discussion started: 26 November 2026
© Author(s) 2026. CC BY 4.0 License.



eawe european academy of wind energy
Open Access WIND ENERGY SCIENCE DISCUSSIONS

Both simulations reproduce the LLJ approaching the double ridge from the southwest, and the simulated wind are in principle consistent with observations. However, the jet structure and especially the near-surface layers differ substantially between runs adopting different z_0. In the CTRL case (Figure 6a), wind speeds near the surface are overestimated within the valley and above the ridges, as also confirmed by ISFS tower data (Figure 6d, Table S2). Flow separation is not well captured, and recirculation zones are too weak or absent. In contrast, lidar observations (Figure 6c) clearly show flow separation and recirculation in the lee of the upwind ridge, characterized by flow reversal against the prevailing wind, feature that is reproduced in MOD (Figure 6b). Radiosonde wind speeds at the launch site also agree more closely with MOD, although the approximately one-hour difference between the lidar composite (04:01 UTC) and the radiosonde launch (05 UTC) should be considered when comparing the observations. These findings highlight the importance of surface friction in shaping the structure and wavelength of trapped lee waves.

An additional point is that finer vertical resolution does not always guarantee improved results: despite CTRL uses a higher number of vertical levels in d05 ($N_z = 109$) compared with MOD ($N_z = 75$), it fails to capture key flow features. The jet structure and near-surface flow in MOD agree better with lidar data, with reduced surface winds, the development of recirculation zones that more closely match observations. By contrast, CTRL fails to reproduce the interaction between the LLJ and the double-ridge topography, leading to an elevated jet and locally stronger winds aloft rather than near the surface.

Figure S5 shows cross-sections at 0510 UTC on each simulation day, corresponding to the radiosonde launch time, to analyze wind flow patterns across different days. Overall, MOD profiles (Figure S5b, e, and h) show better agreement with radiosonde and ISFS observations (Figure S5c, f, and i, Table S2). An exception occurs on May 20, when CTRL performs better, producing lower errors in wind speed within the valley and at the radiosonde site. On May 20 and 21, both simulations reproduce a northeasterly LLJ approaching the ridges, with maximum wind speeds over the southwestern ridge (tse04). For MOD, this case yields the lowest bias and RMSE for wind speed up to 100 m (Table S2).

Moreover, recirculation zones were repeatedly observed in Perdigão under both southwesterly and northeasterly wind directions and have been analyzed in detail using lidar observations (Menke et al., 2019). In this study, we present two representative examples from the simulation period, one for each wind regime. Figure 7a-b illustrates the northeasterly case, averaged over 15 minutes between 15:30 and 15:45 UTC on 19 May, while the southwesterly case (shown in the Supplementary Material, Figure S6) corresponds to 18:20–18:35 UTC on 21 May. In CTRL (Figures 7a and S6a), the lack of realistic z_0 (absence of forest, i.e., non-representative z_0) suppresses proper flow separation and weakens the development of recirculation zones in the valley and along the lee slopes of the ridges. In contrast, MOD (Figures 7b and S6b) exhibits stronger flow reversal and enhanced turbulence, as indicated by TKE (Figures 7c and d and S6c and d), particularly near the ridges and within the valley (highlighted by the white boxes). These simulated features are consistent with lidar observations of recirculation and enhanced turbulence during such events (Menke et al., 2019). To further investigate the sensitivity of the resolved turbulence structure to the surface modifications, Figures S7 and S8 present vertical profiles of the resolved velocity variances ($\overline{u'^2}$, $\overline{v'^2}$, and $\overline{w'^2}$) and Reynolds stresses ($\overline{u'w'}$ and $\overline{v'w'}$) for CTRL and MOD during the two representative wind periods. The profiles are horizontally averaged over three representative regions along the cross-section: the windward slope, valley, and downwind slope. Across both wind regimes, clear differences between CTRL and MOD are evident in the magnitude and vertical distribution of the velocity

https://doi.org/10.5194/wes-2026-216
Preprint. Discussion started: 26 November 2026
© Author(s) 2026. CC BY 4.0 License.

variances, demonstrating that the surface modifications affect not only the overall turbulence magnitude represented by TKE, but also the component-wise structure of the resolved turbulence. In general, MOD exhibits enhanced velocity variances over substantial portions of the lower atmosphere, although the magnitude and vertical extent of these differences depend strongly on height, terrain location, and wind regime. Pronounced differences are also evident in $\overline{u'w'}$ and $\overline{v'w'}$, indicating substantial modifications to the vertical transport of horizontal momentum. The magnitude and, in some regions, the sign of the Reynolds stresses differ between CTRL and MOD and vary with height and terrain position, highlighting the spatially heterogeneous response of the turbulence structure associated with flow separation and recirculation over the complex terrain.

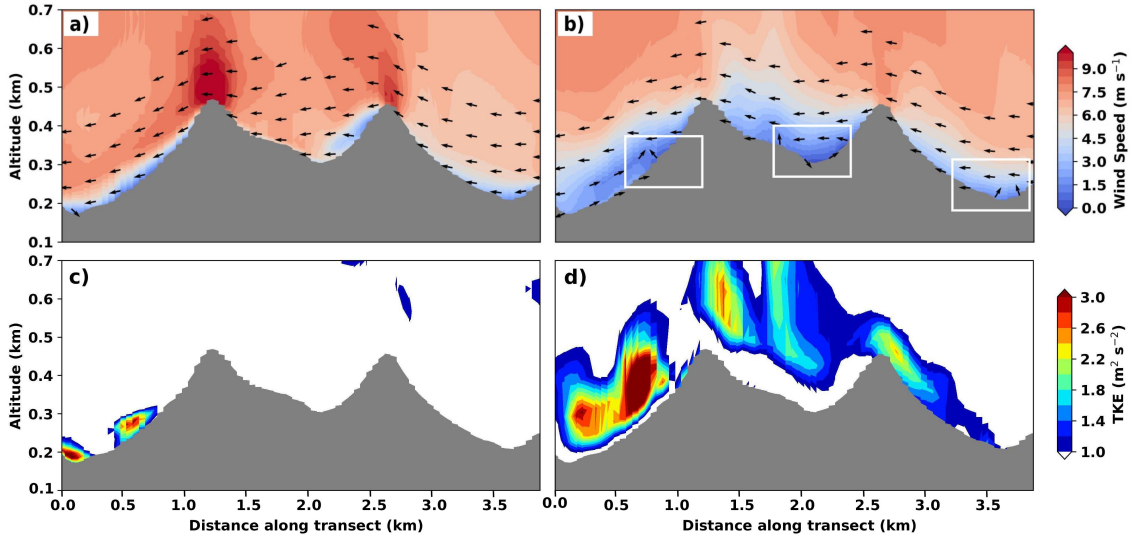


Figure 7. Cross-sections of wind speed (shaded, m s^{-1}; panels a–b), and turbulent kinetic energy (TKE, m^2 s^{-2}; panels c–d), averaged over 15 minutes between 15:30 and 15:45 UTC on 19 May. The left column (a, c) corresponds to the CTRL run, while the right column (b, d) shows the MOD run. Black arrows indicate the flow direction. White boxes highlight regions of flow reversal and enhanced turbulence. In the TKE panels, values below 1 m^2 s^{-2} are shown in white.

To complement the analysis of resolved turbulence during the two representative wind periods, we evaluate the simulated turbulence diagnostics against ISFS observations over the entire four-day study period. Figure 8 presents vertical profiles of $\overline{u'^2_{\parallel}}$, $\overline{w'^2}$, and TKE at three representative towers (tse04, tse09, and tse13). The profiles represent the mean of the hourly diagnostics, with horizontal error bars indicating ± 1 standard deviation. CTRL systematically overestimates all three diagnostics, whereas MOD shows closer agreement with observations across the three towers, particularly for $\overline{w'^2}$. These findings are supported by the quantitative evaluation in Table S4, which shows that MOD reduces the RMSE for all three diagnostics at all evaluated towers and heights. Averaged across the 15 tower–height combinations, the RMSE decreases by approximately 24%, 65%, and 40% for $\overline{u'^2_{\parallel}}$, $\overline{w'^2}$, and TKE, respectively. While MOD reduces the four-day mean turbulence diagnostics, it locally enhances resolved turbulence during recirculation events, reflecting the different spatial and temporal scales characterized by the two analyses. Overall, the surface modifications in MOD alter the intensity and vertical structure of resolved turbulence, with a

https://doi.org/10.5194/wes-2026-216
Preprint. Discussion started: 26 November 2026
© Author(s) 2026. CC BY 4.0 License.

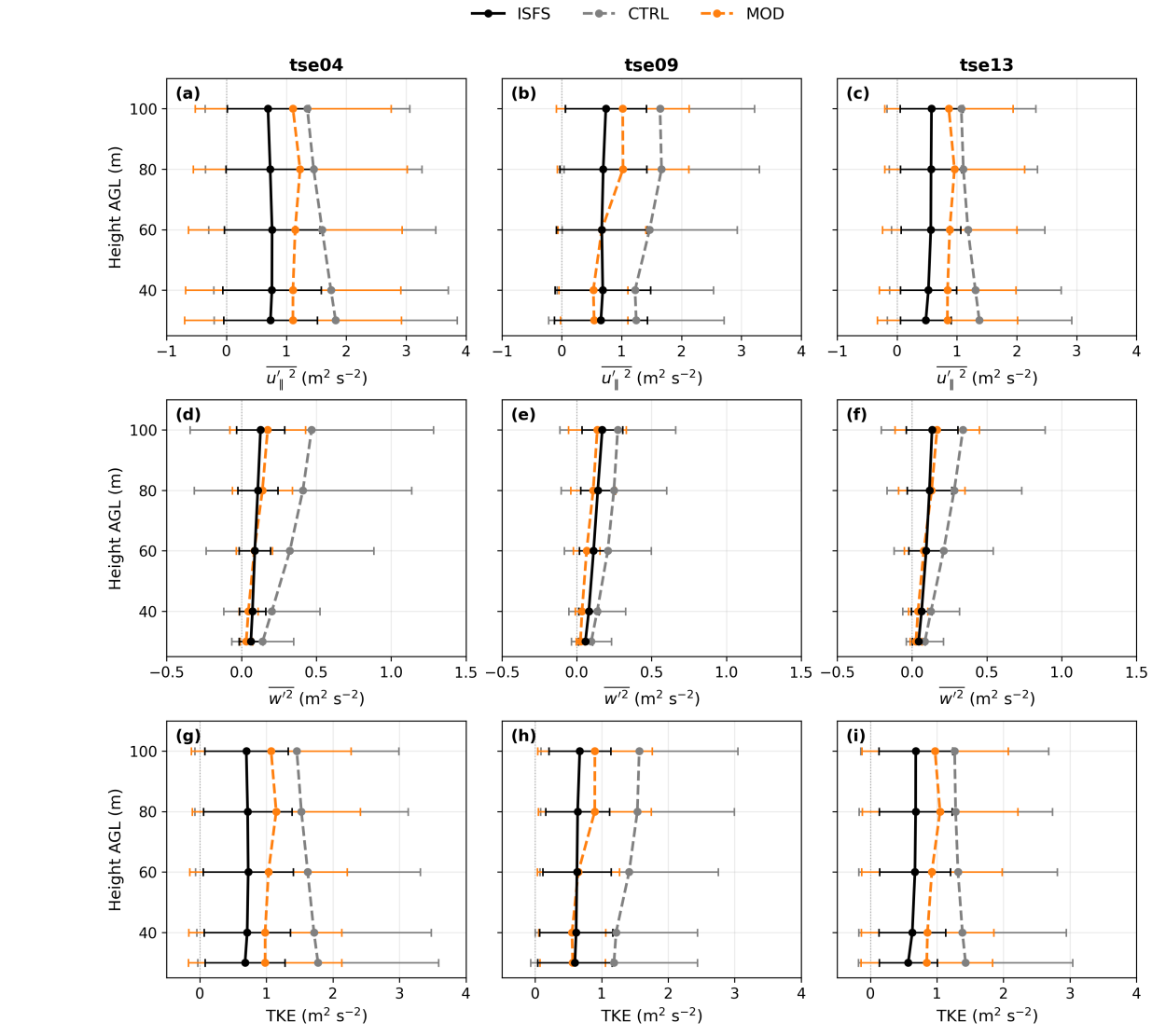


Figure 8. Vertical profiles of $\overline{u'^2_\parallel}$ (a–c), $\overline{w'^2}$ (d–f), and TKE (g–i) from ISFS observations (black), CTRL (gray), and MOD (orange) at towers tse04 (left), tse09 (middle), and tse13 (right). The profiles represent the mean of the matched hourly diagnostics over 19–22 May 2017, and the horizontal error bars indicate ± 1 standard deviation of the hourly values.

These findings are also relevant to wind-energy applications in complex terrain, where accurate simulations of wind speed, vertical wind shear, turbulence, and flow separation is important for characterizing the atmospheric conditions experienced by wind turbines. In particular, errors in simulated wind speed can have substantial implications for wind-power estimates, as

https://doi.org/10.5194/wes-2026-216
Preprint. Discussion started: 26 November 2026
© Author(s) 2026. CC BY 4.0 License.



eawe european academy of wind energy
Open Access WIND ENERGY SCIENCE DISCUSSIONS

the available wind power is proportional to the cube of wind speed De Moliner et al. (2024). The differences between CTRL and MOD demonstrate that surface representation can influence not only near-surface wind magnitudes but also the vertical structure and spatial variability of the flow. The closer agreement with observations of the low-level jet and recirculation zones in MOD further highlights the importance of accounting for forest-induced surface drag when simulating atmospheric flow over complex terrain. These improvements, including the reduced discrepancies between simulated and observed wind profiles up to 100 m AGL, may contribute to more reliable high-resolution wind-resource assessments and characterization of turbine inflow conditions, although their effects on actual turbine power production and loads are not directly evaluated in this study.

3.3 Roughness length influence on other meteorological variables

Surface roughness is a critical parameter in the WRF model, influencing not only wind speed, but also broader land–atmosphere interactions. Z_0 directly controls surface drag and turbulence generation within the planetary boundary layer, thereby shaping temperature, humidity, and momentum fluxes. This section compares CTRL and MOD simulations against ISFS observations, focusing on 2 m temperature and 2 m relative humidity, and potential temperature at 10m and 100 m, in order to assess how z_0 influences model biases and variability.

The model results of surface variables generally agree well with the observations for both near surface relative humidity and air temperature (Figures S9a, S9b). However, errors still occur and are influenced by the model's ability to represent structures in the lower boundary layer over complex terrain. For relative humidity, the two runs are almost identical, with negligible differences except during late May 21 into May 22. In this period, weaker synoptic winds reached the area and facilitated wind veering (Al Oqaily et al., 2025). The transition from strong to weaker winds likely caused the relative humidity to drop in the simulations, but not in the observations (Figure S9a). The small differences between the two runs are limited to this period; overall, they agree well, and changes in z_0 have little effect on 2 m relative humidity. Figure 9a also shows no difference in the MB spatial variability across the ISFS towers. For temperature, both runs also agree well with the observations, but they show a daytime cold bias, except during the peak on May 21. Under strong synoptic forcing, the usual day–night cycle of model errors is not seen, and the errors depend more on the flow pattern (Figure S9b). Most of the thermal response to the z_0 change occurs at the land–atmosphere interface, while the air temperature stays relatively stable, with only a small MB difference of about 0.34°C from CTRL (Figure S9b). This suggests that most adjustments in energy balance remain at the surface, with little influence on the near-surface air, as further discussed in Section 3.4. Moreover, the MB spatial variability between the ISFS towers is nearly the same in both runs (Figure 9b).

The vertical gradient of potential temperature is closely linked to surface heat fluxes, as it reflects the stability of the lower atmosphere and the efficiency of turbulent transport. At 10 m, potential temperature in MOD agrees well with observations, with a mean bias (MB) of 0.38 K, compared to a larger MB of 3.58 K in CTRL (Figure S9c). At 100 m, however, both runs show good agreement with observations, with MB and RMSE values that are nearly identical (Figure S9d). These results suggest that changes in z_0 primarily affect fluxes and temperature structure close to the surface, while higher levels remain largely unaffected.

https://doi.org/10.5194/wes-2026-216
Preprint. Discussion started: 26 November 2026
© Author(s) 2026. CC BY 4.0 License.

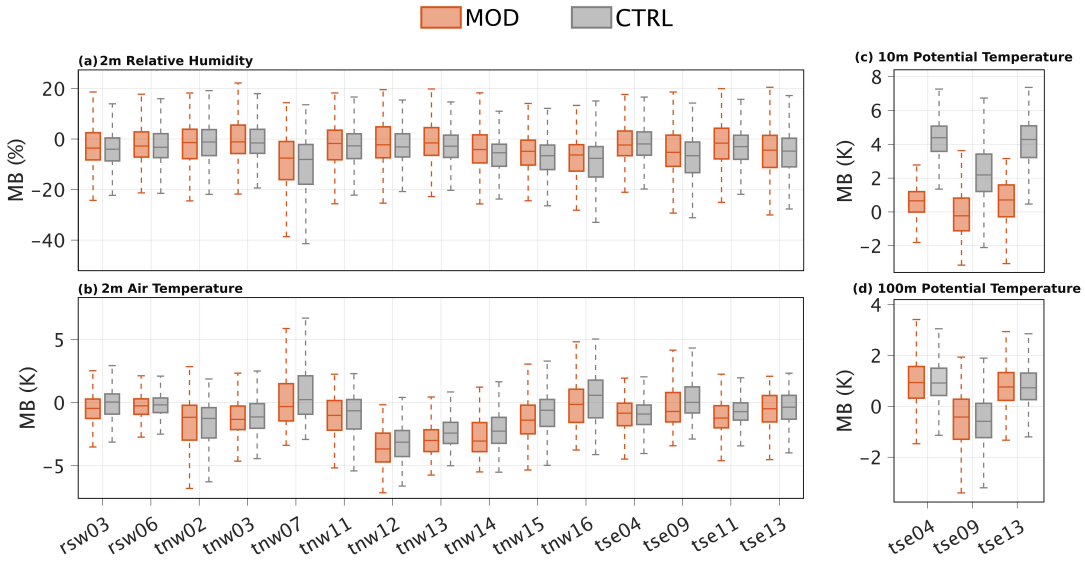


Figure 9. Boxplots of mean bias (MB) comparing CTRL (gray) and MOD (orange) simulations against ISFS observations at tower locations. The spread in each boxplot represents the variability in the 5-min values over four days at each location, labeled as "r" for ridge towers and "t" for transect towers. Panels show: (a) 2 m relative humidity (MB in %), (b) 2 m air temperature (MB in K), (c) 10 m potential temperature (MB in K), and (d) 100 m potential temperature (MB in K).

3.4 Surface Energy Budget and Heat Fluxes

The MOD simulation adopts a different land-use category, resulting in lower domain-averaged daytime albedo (0.12) compared with CTRL (0.22), consistent with the vegetation parameters prescribed by the WRF look-up table (VEGPARM.TBL; Table S3). This difference in albedo directly affects SW_{net}, as shown in Equation 5. Consequently, MOD absorbs more incoming shortwave radiation, with an average increase in SW_{net} of approximately 53 W m^{-2} (Figure 10a). This contributes to an increase in net radiation (R_{net}) of approximately 66 W m^{-2} relative to CTRL (Table S3). These differences are calculated over the daytime period (06:00–20:00 UTC) on 20 May, when differences in the surface energy budget are most pronounced.

Despite the increase in absorbed solar radiation, MOD exhibits lower daytime TSK, with an average reduction of approximately 2 K compared with CTRL (Figure 10b; Table S3). The largest differences occur near peak daytime heating, while nighttime temperatures remain nearly unchanged. This cooling is consistent with more efficient turbulent heat exchange between the surface and atmosphere associated with the modified surface representation. In particular, increased z_0 may enhance the turbulent heat transfer coefficient (C_h), allowing more efficient sensible heat transfer for a smaller surface–air temperature difference. The sensible heat flux can be expressed as $H = \rho C_p C_h U(TSK - \theta_a)$ (Jiménez et al., 2012), where U is the near-surface wind speed and θ_a is the near-surface air potential temperature. Although TSK decreases in MOD, near-surface air

https://doi.org/10.5194/wes-2026-216
Preprint. Discussion started: 26 November 2026
© Author(s) 2026. CC BY 4.0 License.

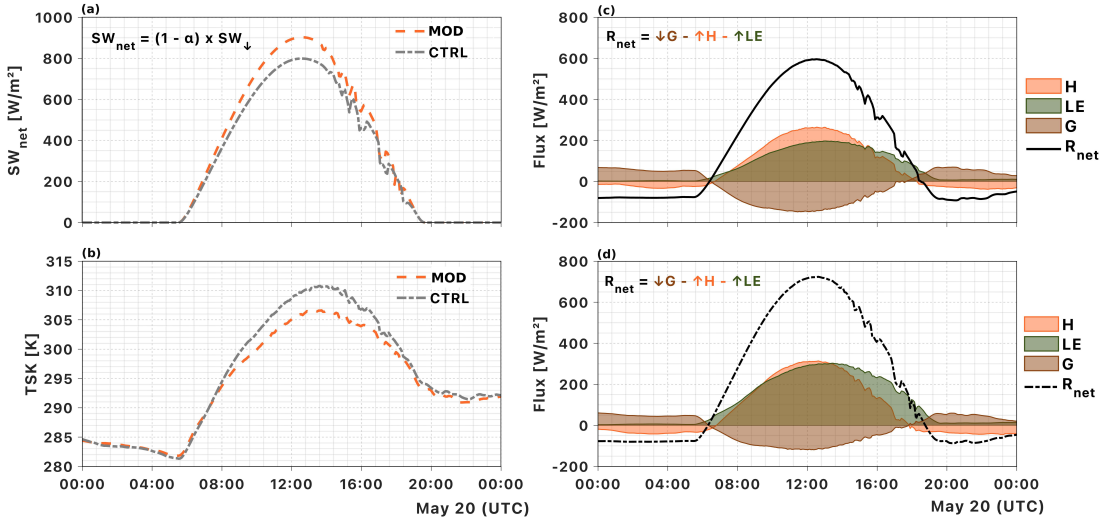


Figure 10. Diurnal variation of surface energy budget components on May 20 for CTRL and MOD simulations over the LES domain (d05). (a) Net shortwave (SW) radiation. (b) Surface skin temperature (TSK). (c) Energy flux partitioning for CTRL: sensible heat flux (H), latent heat flux (LE), and ground heat flux (G) stacked beneath net radiation (R_{net}). (d) Same as (c) but for MOD.

temperature remains nearly unchanged between the simulations (Figure S9b), reducing the surface–air temperature difference. Nevertheless, daytime H increases by an average of 20.35 W m^{-2} in MOD (Table S3). This suggests that changes in the turbulent heat transfer coefficient and near-surface wind speed, together with the greater available radiative energy, may compensate for the smaller temperature difference. However, because C_h was not explicitly diagnosed, its individual contribution cannot be quantified.

The increase in turbulent energy exchange is also reflected in LE, which increases by an average of 53.51 W m^{-2} in MOD relative to CTRL (Table S3). Meanwhile, G decreases by 8.62 W m^{-2} during daytime hours. Together, these changes are consistent with the approximately 66 W m^{-2} increase in R_{net}, indicating a redistribution of the additional available energy toward turbulent heat fluxes (Figure 10c,d). The enhanced H and LE are consistent with the lower daytime TSK, despite the increased absorption of shortwave radiation associated with the lower albedo. These responses likely reflect the combined influence of z_0 and other modified vegetation properties, rather than changes in z_0 alone.

To evaluate the simulated surface radiation components against observations, we used measurements from the three ISFS towers (rne01, rsw04, and v04) which have surface radiation measurements. The mean bias in SW_{net} is 3.7 W m^{-2} for MOD, compared with -30.1 W m^{-2} for CTRL, indicating that the lower albedo in MOD improves agreement with the observed shortwave radiation budget. Figure 11 compares the simulated and observed R_{net} from May 19 to May 22. The MOD simulation closely follows the observed diurnal variations, with a mean bias of 1.6 W m^{-2}, compared with -40.1 W m^{-2} for CTRL. These results indicate that MOD better reproduces the observed surface radiation budget, particularly SW_{net} and R_{net}.

https://doi.org/10.5194/wes-2026-216
Preprint. Discussion started: 26 November 2026
© Author(s) 2026. CC BY 4.0 License.



eawe european academy of wind energy
Open Access WIND ENERGY SCIENCE DISCUSSIONS

However, the differences in H and LE between the simulations represent changes in the modeled responses to the modified surface properties and were not independently evaluated against observations.

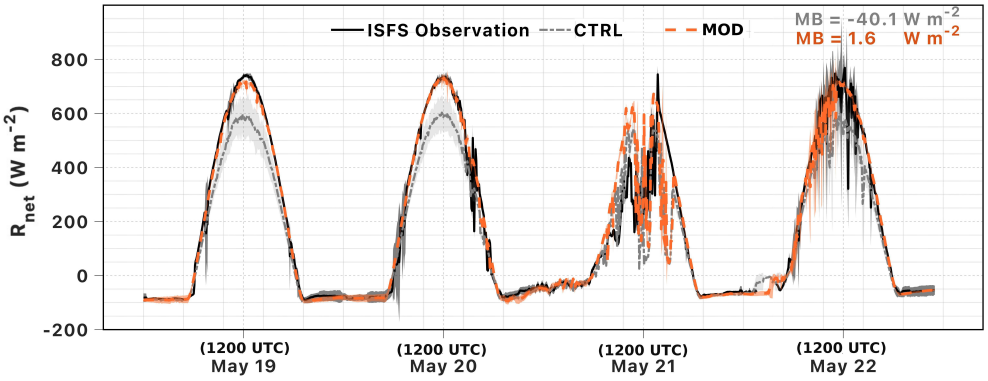


Figure 11. Time series of net radiation R_{net} from ISFS observations (black), *CTRL* simulation (gray dash-dot), and *MOD* simulation (orange dashed) from May 19 to May 22, averaged across three towers (rne01, rsw04, and v04) where ISFS data are available. Shaded areas represent the spread in ISFS towers. The mean bias relative to observations is indicated on the right: -40.1 W m^{-2} for *CTRL* and $+1.6$ W m^{-2} for *MOD*.

Overall, the surface energy budget analysis shows that MOD produces lower daytime surface temperatures despite increased R_{net}, accompanied by enhanced H and LE. This response is consistent with more efficient surface–atmosphere energy exchange associated with the modified surface representation. However, these differences reflect the combined effects of changes in land-surface properties and vertical-grid configuration, rather than the isolated influence of z_0.

4 Conclusions

In this study, four WRF-LES simulations were conducted to investigate the influence of surface representation and vertical grid resolution on microscale boundary-layer flow during a four-day dry period of the Perdigão 2017 field campaign. The sensitivity experiments examined the effects of vertical grid resolution, z_0, and land-use representation on simulated wind fields. The CTRL and MOD configurations were further compared to assess the combined influence of these modifications on boundary-layer dynamics and surface energy exchange. CTRL uses the default land-use configuration provided by the CORINE dataset, whereas MOD employs a modified surface representation designed to better reflect the forested canopy conditions at the site. This modification includes adjustments to land-surface parameters such as z_0 and the use of vegetation characteristics associated with the forest land-use category, including albedo, LAI, and emissivity, within the LES-resolution domains informed by observations. The results are evaluated through observational and statistical verification using meteorological tower measurements, radiosonde profiles, and lidar cross-sections.

https://doi.org/10.5194/wes-2026-216
Preprint. Discussion started: 26 November 2026
© Author(s) 2026. CC BY 4.0 License.



eawe european academy of wind energy
Open Access WIND ENERGY SCIENCE DISCUSSIONS

The diurnal cycle during the study period shows a notable improvement in wind speed across all tower locations, particularly on ridge locations, when using z_0 that matches observations. MOD better captures the observed wind speeds throughout the lower boundary layer, with performance improving with height compared to CTRL. However, both simulations exhibit larger errors at night under stable conditions compared to daytime and the synoptic transition period. Increasing Z_0 not only reduces wind magnitudes but also alters wind patterns and flow structures, particularly over complex terrain. In the MOD simulation, the LLJ structure and near-surface flow show better agreement with lidar observations, characterized by weaker surface winds and the development of recirculation zones that more closely match the measurements. In contrast, CTRL fails to capture the interaction between the LLJ and the double-ridge topography, resulting in an elevated jet and locally stronger winds aloft rather than near the surface. Furthermore, MOD exhibits stronger flow reversal and enhanced turbulence, especially near the upwind and downwind ridges and within the valley.

Moreover, z_0 plays a crucial role in regulating land–atmosphere interactions within the WRF-LES model, influencing not only wind speed but also the surface energy balance. The results demonstrate that increasing Z_0 and reducing albedo to better represent the Perdigão canopy significantly modify near-surface fluxes and temperature structure, with the strongest temperature response near the surface and comparatively small differences in potential temperature at 100 m above ground level. The enhanced z_0 strengthens turbulence and surface drag, alters the partitioning of available energy among H, and LE, and increases net radiative flux due to the lower albedo of forests. These findings underscore the importance of accurately representing land surface parameters, particularly z_0 and albedo, in microscale boundary-layer simulations over complex terrain.

Given the high sensitivity of modeled surface wind speed to z_0, realistic surface representation is particularly critical in high-resolution LES, where typical land-use datasets and predefined surface properties are often inadequate. While traditional numerical weather prediction models can rely on averaged roughness and other land-surface parameters over large domains, simulations designed to resolve microscale flow within small domains (e.g., 6×6 km^2) require carefully adjusted values of z_0, albedo, LAI, and canopy height to realistically capture near-surface flow and energy exchange. Although several parameters are modified in MOD, the results indicate that the increase in z_0 represents the dominant factor controlling the improvement in wind speed and turbulence representation. Nevertheless, modifying the entire land-use category ensures a more physically consistent description of canopy properties and their influence on land–atmosphere interactions.

Perdigão site presents unique characteristics, including a double-ridge topography, forest canopy, and strong thermally driven flows, which influence the detailed structure of the simulated boundary-layer dynamics. While some flow features (e.g., the precise structure of recirculation zones and the interaction between the LLJ and the valley geometry) are likely site specific, the broader modeling implications are expected to extend to other forested complex-terrain environments. However, the present modeling framework does not include an explicit canopy-drag parameterization and is therefore not intended to resolve turbulence and momentum exchange within the forest canopy. Consequently, the improved performance obtained when the first model level is located above the canopy should be interpreted as a more physically consistent application of the surface-layer parameterization rather than an explicit improvement in the representation of in-canopy flow. The approach may therefore be less suitable for applications requiring accurate wind predictions within the canopy or in the lowest tens of meters above the surface, such as drone operations, forest-canopy transport studies, or very-low-level aviation. In particular, the strong sensi-

https://doi.org/10.5194/wes-2026-216
Preprint. Discussion started: 26 November 2026
© Author(s) 2026. CC BY 4.0 License.



eawe european academy of wind energy
Open Access WIND ENERGY SCIENCE DISCUSSIONS

tivity of near-surface winds to z_0 representation demonstrated in this study is likely relevant for many mountainous regions with significant vegetation cover. An additional source of uncertainty is associated with the Shin–Hong turbulence closure used in the gray-zone domains, which may affect the representation of subgrid momentum transport, particularly under stable and strongly sheared conditions. Although the same parameterization is applied across all experiments, potential interactions with the modified surface properties cannot be excluded. Future studies could investigate the sensitivity of simulated momentum and moisture fluxes to alternative turbulence parameterizations. Finally, from a wind-energy perspective, these findings emphasize the importance of realistic surface representation when applying high-resolution atmospheric models to forested complex terrain. The substantial reduction in wind-speed errors the ability of MOD to capture complex flow structures suggest that carefully selected z_0 parameters can enhance the reliability of simulated wind conditions relevant to wind-resource assessment and turbine inflow characterization. Although the present study does not directly evaluate wind power production or turbine performance, it identifies surface representation as an important source of uncertainty that should be considered in future wind-energy modeling applications over complex terrain.

Code and data availability. The dataset used in this study is openly available via Zenodo at (Al-oqaily, 2026). It includes wind components, and energy budget components from WRF simulations driven by different land use category, along with the main figure-generation codes. The namelist of the simulation ensemble is also included at the same Zenodo. Data analysis and visualization were conducted using MATLAB R2024b (The MathWorks, Inc., 2024) and Python 3.12.6 (Van Rossum and Drake, 2009). Integrated Surface Flux System are obtained from UCAR/NCAR - Earth Observing Laboratory (EOL) (UCAR/NCAR - Earth Observing Laboratory, 2019), Radiosonde data are also obtained from UCAR/NCAR - Earth Observing Laboratory (UCAR/NCAR - Earth Observing Laboratory, 2018). The DTU lidar data are provided by (Menke et al., 2019). CORINE land cover data are obtained from Copernicus (European Environment Agency, 2002), and SRTM data are obtained from USGS https://doi.org/10.5066/F7F76B1X. Initial and boundary conditions data for simulations are obtained from NCAR's Research Data Archive https://rda.ucar.edu/datasets/d633000/ for ERA5.

Author contributions. DA: conceptualization, data curation, formal analysis, investigation, methodology, software, validation, visualization, and writing (original draft, review and editing). PG: conceptualization, methodology, and writing (review and editing). PC: funding acquisition, supervision, conceptualization, methodology, resources, and writing (review and editing).

Competing interests. The authors declare no competing interests relevant to this study.

Acknowledgements. This study is based upon work supported by the National Science Foundation under Grants No. 2236504 and No. 2213579 to PC, as well as the King Abdullah University of Science and Technology (KAUST) Office of Sponsored Research (OSR) under Award ORFS-2022-CRG11-5069.2 to PC.

https://doi.org/10.5194/wes-2026-216
Preprint. Discussion started: 26 November 2026
© Author(s) 2026. CC BY 4.0 License.



eawe european academy of wind energy
Open Access WIND ENERGY SCIENCE DISCUSSIONS

References

Adedipe, T. A., Chaudhari, A., and Kauranne, T.: Impact of different forest densities on atmospheric boundary-layer development and wind-turbine wake, Wind Energy, 23, 1165–1180, https://doi.org/10.1002/we.2464, 2020.

Agafonova, O.: A numerical study of forest influences on the atmospheric boundary layer and wind turbines, Ph.D. thesis, Lappeenranta University of Technology, Lappeenranta, Finland, ISBN 978-952-335-110-3, https://lutpub.lut.fi/handle/10024/143223, 2017.

Al-oqaily, D.: WRF Simulations Configurations, Dataset and Codes, https://doi.org/10.5281/zenodo.24517805, 2026.

Al Oqaily, D., Giani, P., and Crippa, P.: Evaluating WRF multiscale wind simulations in complex terrain: Insights from the Perdigão field campaign, Journal of Geophysical Research: Atmospheres, 130, e2025JD044 055, https://doi.org/10.1029/2025JD044055, 2025.

Arthur, R. S., Mirocha, J. D., Lundquist, K. A., and Street, R. L.: Using a canopy model framework to improve large-eddy simulations of the neutral atmospheric boundary layer in the Weather Research and Forecasting model, Monthly Weather Review, 147, 31–52, https://doi.org/10.1175/MWR-D-18-0204.1, 2019.

Arya, P. S.: Introduction to micrometeorology, vol. 79, Elsevier, https://www.sciencedirect.com/bookseries/international-geophysics/vol/79/suppl/C, 2001.

Aumond, P., Masson, V., Lac, C., Gauvreau, B., Dupont, S., and Berengier, M.: Including the drag effects of canopies: real case large-eddy simulation studies, Boundary-layer meteorology, 146, 65–80, https://doi.org/10.1007/s10546-012-9758-x, 2013.

Auvinen, M., Boi, S., Hellsten, A., Tanhuanpää, T., and Järvi, L.: Study of realistic urban boundary layer turbulence with high-resolution large-eddy simulation, Atmosphere, 11, 201, https://doi.org/10.3390/atmos11020201, 2020.

Banta, R. M., Darby, L. S., Fast, J. D., Pinto, J. O., Whiteman, C. D., Shaw, W. J., and Orr, B. W.: Nocturnal low-level jet in a mountain basin complex. Part I: Evolution and effects on local flows, Journal of applied meteorology, 43, 1348–1365, https://doi.org/10.1175/JAM2142.1, 2004.

Basu, S. and Porté-Agel, F.: Large-eddy simulation of stably stratified atmospheric boundary layer turbulence: a scale-dependent dynamic modeling approach, Journal of the Atmospheric Sciences, 63, 2074–2091, https://doi.org/10.1175/JAS3734.1, 2006.

Bonan, G. B., Patton, E. G., Harman, I. N., Oleson, K. W., Finnigan, J. J., Lu, Y., and Burakowski, E. A.: Modeling canopy-induced turbulence in the Earth system: A unified parameterization of turbulent exchange within plant canopies and the roughness sublayer (CLM-ml v0), Geoscientific Model Development, 11, 1467–1496, https://doi.org/10.5194/gmd-11-1467-2018, 2018.

Daniels, M. H., Lundquist, K. A., Mirocha, J. D., Wiersema, D. J., and Chow, F. K.: A new vertical grid nesting capability in the Weather Research and Forecasting (WRF) Model, Monthly Weather Review, 144, 3725–3747, https://doi.org/10.1175/MWR-D-16-0049.1, 2016.

De Meij, A., Gzella, A., Cuvelier, C., Thunis, P., Bessagnet, B., Vinuesa, J., Menut, L., and Kelder, H.: The impact of MM5 and WRF meteorology over complex terrain on CHIMERE model calculations, Atmospheric Chemistry and Physics, 9, 6611–6632, https://doi.org/10.5194/acp-9-6611-2009, 2009.

De Moliner, G., Giani, P., Lonati, G., and Crippa, P.: Sensitivity of multiscale large Eddy simulations for wind power calculations in complex terrain, Applied Energy, 364, 123 195, https://doi.org/10.1016/j.apenergy.2024.123195, 2024.

Deardorff, J. W.: Stratocumulus-capped mixed layers derived from a three-dimensional model, Boundary-layer meteorology, 18, 495–527, https://doi.org/10.1007/BF00119502, 1980.

Dudhia, J.: Numerical study of convection observed during the winter monsoon experiment using a mesoscale two-dimensional model, Journal of Atmospheric Sciences, 46, 3077–3107, https://doi.org/10.1175/1520-0469(1989)046<3077:NSOCOD>2.0.CO;2, 1989.

https://doi.org/10.5194/wes-2026-216
Preprint. Discussion started: 26 November 2026
© Author(s) 2026. CC BY 4.0 License.

Dupont, S. and Brunet, Y.: Impact of forest edge shape on tree stability: a large-eddy simulation study, Forestry, 81, 299–315, https://doi.org/10.1093/forestry/cpn006, 2008.

Ek, M., Mitchell, K., Lin, Y., Rogers, E., Grunmann, P., Koren, V., Gayno, G., and Tarpley, J.: Implementation of Noah land surface model advances in the National Centers for Environmental Prediction operational mesoscale Eta model, Journal of Geophysical Research: Atmospheres, 108, https://doi.org/10.1029/2002JD003296, 2003.

Elgendi, M., AlMallahi, M., Abdelkhalig, A., and Selim, M. Y.: A review of wind turbines in complex terrain, International Journal of Thermofluids, 17, 100 289, https://doi.org/10.1016/j.ijft.2023.100289, 2023.

European Environment Agency: Corine land cover 2000. Technical guidelines, https://www.eea.europa.eu/en/analysis/publications/tech40add, 2002.

Fang, J., Peringer, A., Stupariu, M.-S., Pătru-Stupariu, I., Buttler, A., Golay, F., and Porté-Agel, F.: Shifts in wind energy potential following land-use driven vegetation dynamics in complex terrain, Science of the Total Environment, 639, 374–384, https://doi.org/10.1016/j.scitotenv.2018.05.083, 2018.

Fernando, H., Mann, J., Palma, J., Lundquist, J. K., Barthelmie, R. J., Belo-Pereira, M., Brown, W., Chow, F., Gerz, T., Hocut, C., et al.: The Perdigão: peering into microscale details of mountain winds, Bulletin of the American Meteorological Society, 100, 799–819, https://doi.org/10.1175/BAMS-D-17-0227.1, 2019.

Giani, P. and Crippa, P.: On the Sensitivity of Large-Eddy Simulations of the Atmospheric Boundary Layer Coupled with Realistic Large-Scale Dynamics, Monthly Weather Review, 152, 1057–1075, https://doi.org/10.1175/MWR-D-23-0101.1, 2024.

Giani, P., Genton, M. G., and Crippa, P.: Modeling the convective boundary layer in the terra incognita: Evaluation of different strategies with real-case simulations, Monthly Weather Review, 150, 981–1001, https://doi.org/10.1175/MWR-D-21-0216.1, 2022.

Harman, I. N. and Finnigan, J. J.: A simple unified theory for flow in the canopy and roughness sublayer, Boundary-layer meteorology, 123, 339–363, https://doi.org/10.1007/s10546-006-9145-6, 2007.

Hersbach, H., Bell, B., Berrisford, P., Hirahara, S., Horányi, A., Muñoz-Sabater, J., Nicolas, J., Peubey, C., Radu, R., Schepers, D., et al.: The ERA5 global reanalysis, Quarterly Journal of the Royal Meteorological Society, 146, 1999–2049, https://doi.org/10.1002/qj.3803, [Dataset], 2020.

Hung, W.-T., Campbell, P. C., Moon, Z., Saylor, R., Kochendorfer, J., Lee, T. R., and Massman, W.: Evaluation of an in-canopy wind and wind adjustment factor model for wildfire spread applications across scales, Journal of Advances in Modeling Earth Systems, 16, e2024MS004 300, https://doi.org/10.1029/2024MS004300, 2024.

Janiszeski, A. and Crippa, P.: Multiscale WRF modeling of meso-to micro-scale flows during Sundowner events, Journal of Geophysical Research: Atmospheres, 130, e2024JD042 972, https://doi.org/10.1029/2024JD042972, 2025.

Jiménez, P. A., Dudhia, J., González-Rouco, J. F., Navarro, J., Montávez, J. P., and García-Bustamante, E.: A revised scheme for the WRF surface layer formulation, Monthly weather review, 140, 898–918, https://doi.org/10.1175/MWR-D-11-00056.1, 2012.

June, T., Meijide, A., Stiegler, C., Kusuma, A., and Knohl, A.: The influence of surface roughness and turbulence on heat fluxes from an oil palm plantation in Jambi, Indonesia. IOP Conf, Ser. Earth Environ. Sci, 149, 1755–1315, https://doi.org/10.1088/1755-1315/149/1/012048, 2018.

Kadivar, M., Tormey, D., and McGranaghan, G.: A review on turbulent flow over rough surfaces: Fundamentals and theories, International Journal of Thermofluids, 10, 100 077, https://doi.org/10.1016/j.ijft.2021.100077, 2021.

Kain, J. S. and Fritsch, J. M.: A one-dimensional entraining/detraining plume model and its application in convective parameterization, Journal of Atmospheric Sciences, 47, 2784–2802, https://doi.org/10.1175/1520-0469(1990)047<2784:AODEPM>2.0.CO;2, 1990.

https://doi.org/10.5194/wes-2026-216
Preprint. Discussion started: 26 November 2026
© Author(s) 2026. CC BY 4.0 License.

Kelly, M. and Jørgensen, H. E.: Statistical characterization of roughness uncertainty and impact on wind resource estimation, Wind Energy Science, 2, 189–209, https://doi.org/10.5194/wes-2-189-2017, 2017.

Khanna, S. and Brasseur, J. G.: Analysis of Monin–Obukhov similarity from large-eddy simulation, Journal of Fluid Mechanics, 345, 251–286, https://doi.org/10.1017/S0022112097006277, 1997.

Lee, J., Hong, J., Noh, Y., and Jiménez, P. A.: Implementation of a roughness sublayer parameterization in the Weather Research and Forecasting model (WRF version 3.7. 1) and its evaluation for regional climate simulations, Geoscientific Model Development, 13, 521–536, https://doi.org/10.5194/gmd-13-521-2020, 2020.

Lee, J., Lee, H.-J., Kim, K.-B., Shin, H. H., Lim, J.-M., Hong, J., and Lim, K.-S. S.: Height correction method based on the Monin–Obukhov similarity theory for better prediction of near-surface wind fields, Atmospheric Research, 292, 106 882, https://doi.org/10.1016/j.atmosres.2023.106882, 2023.

Liu, Y., Liu, Y., Muñoz-Esparza, D., Hu, F., Yan, C., and Miao, S.: Simulation of flow fields in complex terrain with WRF-LES: Sensitivity assessment of different PBL treatments, Journal of Applied Meteorology and Climatology, 59, 1481–1501, https://doi.org/10.1175/JAMC-D-19-0304.1, 2020.

Liu, Z., Ishihara, T., He, X., and Niu, H.: LES study on the turbulent flow fields over complex terrain covered by vegetation canopy, Journal of Wind Engineering and Industrial Aerodynamics, 155, 60–73, https://doi.org/10.1016/j.jweia.2016.05.002, 2016.

Mahrer, Y.: An improved numerical approximation of the horizontal gradients in a terrain-following coordinate system, Monthly Weather Review, 112, 918–922, https://doi.org/10.1175/1520-0493(1984)112<0918:AINAOT>2.0.CO;2, 1984.

Maronga, B.: Monin–Obukhov similarity functions for the structure parameters of temperature and humidity in the unstable surface layer: Results from high-resolution large-eddy simulations, Journal of the Atmospheric Sciences, 71, 716–733, https://doi.org/10.1175/JAS-D-13-0135.1, 2014.

Menke, R., Vasiljević, N., Mann, J., and Lundquist, J. K.: Characterization of flow recirculation zones at the Perdigão site using multi-lidar measurements, Atmospheric Chemistry and Physics, 19, 2713–2723, https://doi.org/10.5194/acp-19-2713-2019, [Dataset], 2019.

Mirocha, J. D., Lundquist, J. K., and Kosović, B.: Implementation of a nonlinear subfilter turbulence stress model for large-eddy simulation in the Advanced Research WRF model, Monthly Weather Review, 138, 4212–4228, https://doi.org/10.1175/2010MWR3286.1, 2010.

Mlawer, E. J., Taubman, S. J., Brown, P. D., Iacono, M. J., and Clough, S. A.: Radiative transfer for inhomogeneous atmospheres: RRTM, a validated correlated-k model for the longwave, Journal of Geophysical Research: Atmospheres, 102, 16 663–16 682, https://doi.org/10.1029/97JD00237, 1997.

Monin, A. S. and Obukhov, A. M.: Basic laws of turbulent mixing in the surface layer of the atmosphere, Contrib. Geophys. Inst. Acad. Sci. USSR, 151, e187, https://gibbs.science/efd/handouts/monin_obukhov_1954.pdf, 1954.

NCAR: Corrections to Sensible and Latent Heat Flux Measurements, https://www.eol.ucar.edu/content/corrections-sensible-and-latent-heat-flux-measurements, accessed: 2025-07-09, 2025.

Ngan, F., Kim, H., Lee, P., Al-Wali, K., and Dornblaser, B.: A study of nocturnal surface wind speed overprediction by the WRF-ARW model in southeastern Texas, Journal of applied meteorology and climatology, 52, 2638–2653, https://doi.org/10.1175/JAMC-D-13-060.1, 2013.

Nishizawa, S., Yashiro, H., Sato, Y., Miyamoto, Y., and Tomita, H.: Influence of grid aspect ratio on planetary boundary layer turbulence in large-eddy simulations, Geoscientific Model Development, 8, 3393–3419, https://doi.org/10.5194/gmd-8-3393-2015, 2015.

North, G. R., Pyle, J. A., and Zhang, F.: Encyclopedia of atmospheric sciences, vol. 1, Elsevier, https://www.sciencedirect.com/referencework/9780123822253/encyclopedia-of-atmospheric-sciences, 2014.

https://doi.org/10.5194/wes-2026-216
Preprint. Discussion started: 26 November 2026
© Author(s) 2026. CC BY 4.0 License.



Pineda, N., Jorba, O., Jorge, J., and Baldasano, J.: Using NOAA AVHRR and SPOT VGT data to estimate surface parameters: application to a mesoscale meteorological model, International journal of remote sensing, 25, 129–143, https://doi.org/10.1080/0143116031000115201, 2004.

Quimbayo-Duarte, J., Wagner, J., Wildmann, N., Gerz, T., and Schmidli, J.: Evaluation of a forest parameterization to improve boundary layer flow simulations over complex terrain. A case study using WRF-LES V4.0.1, Geoscientific Model Development, 15, 5195–5209, https://doi.org/10.5194/gmd-15-5195-2022, 2022.

Schicker, I., Arnold Arias, D., and Seibert, P.: Influences of updated land-use datasets on WRF simulations for two Austrian regions, Meteorology and Atmospheric Physics, 128, 279–301, https://doi.org/10.1007/s00703-015-0416-y, 2016.

Schotanus, P., Nieuwstadt, F., and De Bruin, H.: Temperature measurement with a sonic anemometer and its application to heat and moisture fluxes, Boundary-Layer Meteorology, 26, 81–93, https://doi.org/10.1007/BF00164332, 1983.

Sertel, E., Robock, A., and Ormeci, C.: Impacts of land cover data quality on regional climate simulations, International Journal of Climatology, 30, 1942–1953, https://doi.org/10.1002/joc.2036, 2010.

Shaw, R. H. and Schumann, U.: Large-eddy simulation of turbulent flow above and within a forest, Boundary-Layer Meteorology, 61, 47–64, https://doi.org/10.1007/BF02033994, 1992.

Shin, H. H. and Hong, S.-Y.: Representation of the subgrid-scale turbulent transport in convective boundary layers at gray-zone resolutions, Monthly Weather Review, 143, 250–271, https://doi.org/10.1175/MWR-D-14-00116.1, 2015.

Skamarock, W. C., Klemp, J. B., Dudhia, J., Gill, D. O., Liu, Z., Berner, J., Wang, W., Powers, J. G., Duda, M. G., Barker, D. M., et al.: A description of the advanced research WRF model version 4, National Center for Atmospheric Research: Boulder, CO, USA, 145, 550, https://doi.org/10.5065/1dfh-6p97, [Software], 2019.

Solbakken, K., Birkelund, Y., and Samuelsen, E. M.: Evaluation of surface wind using WRF in complex terrain: Atmospheric input data and grid spacing, Environmental Modelling & Software, 145, 105 182, https://doi.org/10.1016/j.envsoft.2021.105182, 2021.

Stoll, R. and Porté-Agel, F.: Large-eddy simulation of the stable atmospheric boundary layer using dynamic models with different averaging schemes, Boundary-Layer Meteorology, 126, 1–28, https://doi.org/10.1007/s10546-007-9207-4, 2008.

Storm, B., Dudhia, J., Basu, S., Swift, A., and Giammanco, I.: Evaluation of the weather research and forecasting model on forecasting low-level jets: Implications for wind energy, Wind Energy: An International Journal for Progress and Applications in Wind Power Conversion Technology, 12, 81–90, https://doi.org/10.1002/we.288, 2009.

Stull, R. B.: An introduction to boundary layer meteorology, vol. 13, Springer Science & Business Media, https://doi.org/10.1007/978-94-009-3027-8, 2012.

Szkordilisz, F. and Zöld, A.: Effect of vegetation on wind-comfort, Applied Mechanics and Materials, 824, 811–818, https://doi.org/10.4028/www.scientific.net/AMM.824.811, 2016.

Tamura, T., Okuno, A., and Sugio, Y.: LES analysis of turbulent boundary layer over 3D steep hill covered with vegetation, Journal of Wind Engineering and Industrial Aerodynamics, 95, 1463–1475, https://doi.org/10.1016/j.jweia.2007.02.014, 2007.

The MathWorks, Inc.: MATLAB version R2024b, The MathWorks, Inc., Natick, Massachusetts, https://www.mathworks.com/products/matlab.html, [Software], 2024.

UCAR/NCAR - Earth Observing Laboratory: NCAR/EOL Quality Controlled Radiosonde Data, https://doi.org/10.5065/D6H70DM1, [Dataset] . Accessed March 5, 2025, 2018.

UCAR/NCAR - Earth Observing Laboratory: NCAR/EOL Quality Controlled 5-minute ISFS surface flux data, https://doi.org/10.26023/ZDMJ-D1TY-FG14, [Dataset]. Accessed 05 Mar 2025, 2019.

https://doi.org/10.5194/wes-2026-216
Preprint. Discussion started: 26 November 2026
© Author(s) 2026. CC BY 4.0 License.



Van Rossum, G. and Drake, F. L.: Python 3 Reference Manual, CreateSpace, Scotts Valley, CA, ISBN 1441412697, https://dl.acm.org/doi/book/10.5555/1593511, [Software], 2009.

Venkatraman, K., Hågbo, T.-O., Buckingham, S., and Teigen Giljarhus, K. E.: Effect of different source terms and inflow direction in atmospheric boundary modeling over the complex terrain site of Perdigão, Wind Energy Science, 8, 85–108, https://wes.copernicus.org/articles/8/85/2023/, 2023.

Wagner, J., Gerz, T., Wildmann, N., and Gramitzky, K.: Long-term simulation of the boundary layer flow over the double-ridge site during the Perdigão 2017 field campaign, Atmospheric Chemistry and Physics, 19, 1129–1146, https://doi.org/10.5194/acp-19-1129-2019, 2019a.

Wagner, J., Wildmann, N., and Gerz, T.: Improving boundary layer flow simulations over complex terrain by applying a forest parameterization in WRF, Wind Energy Science Discussions, 2019, 1–25, https://doi.org/10.5194/wes-2019-77, 2019b.

Weber, R. O.: Remarks on the definition and estimation of friction velocity, Boundary-Layer Meteorology, 93, 197–209, https://doi.org/10.1023/A:1002043826623, 1999.

Wise, A. S., Neher, J. M., Arthur, R. S., Mirocha, J. D., Lundquist, J. K., and Chow, F. K.: Meso-to microscale modeling of atmospheric stability effects on wind turbine wake behavior in complex terrain, Wind Energy Science, 7, 367–386, https://wes.copernicus.org/articles/7/367/2022/wes-7-367-2022.pdf, 2022.

Wyngaard, J. C., Peltier, L. J., and Khanna, S.: LES in the surface layer: Surface fluxes, scaling, and SGS modeling, Journal of the Atmospheric Sciences, 55, 1733–1754, https://doi.org/10.1175/1520-0469(1998)055<1733:LITSLS>2.0.CO;2, 1998.